CHALMERS
UNIVERSITY OF TECHNOLOGY

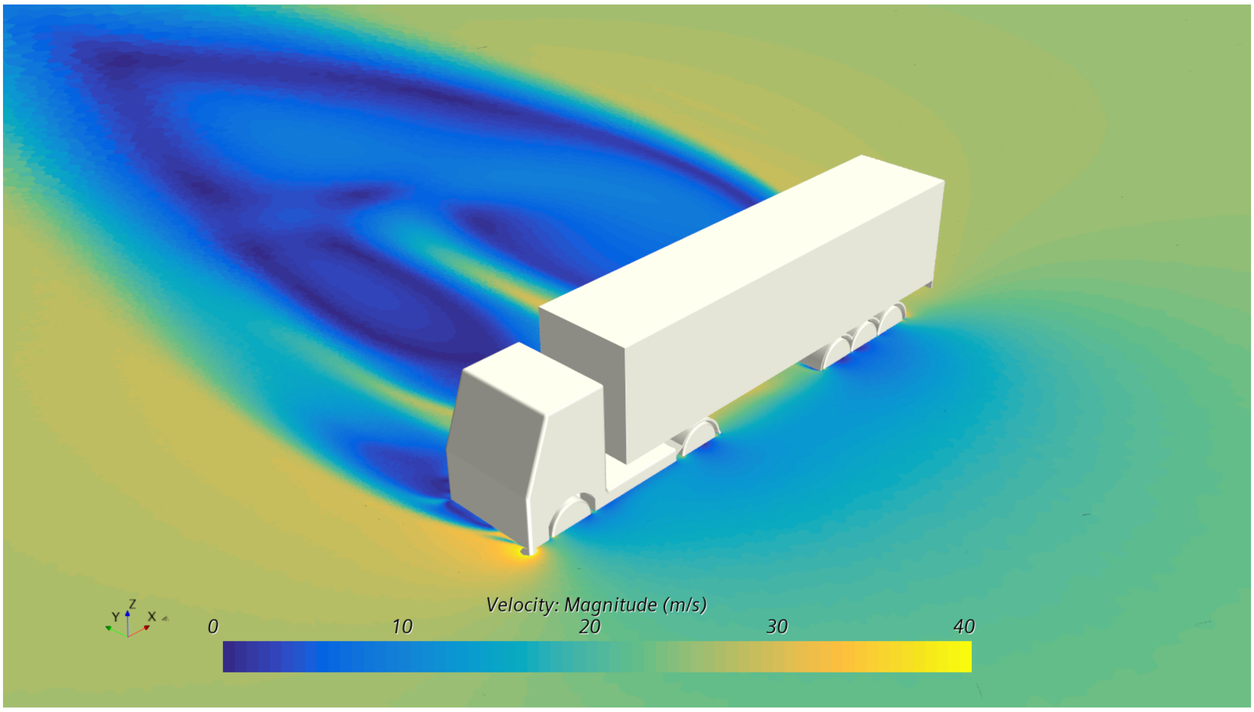

Aerodynamic investigations of a simplified truck under high yaw wind conditions

Final Report

Project in the master Automotive Engineering

Athanasia Dineff
Avaneesh Upadhyaya
Kaushik Nagaraja Rao
Philip van Hoorn
Vinay Gudihal

Department of Mechanics and Maritime Sciences
CHALMERS UNIVERSITY OF TECHNOLOGY
Gothenburg, Sweden 2021

Supervisors: Simone Sebben and Alexey Vdovin
Report number: 2021:02

Department of Mechanics and Maritime Sciences
Division of Fluid Dynamics
Chalmers University of Technology
SE-412 96 Gothenburg
Telephone +46 31 772 1000

Department of Mechanics and Maritime Sciences
Division of Vehicle Engineering and Autonomous Systems (VEAS)
Chalmers University of Technology
Gothenburg, Sweden 2021

Typeset in LaTeX
Gothenburg, Sweden 2021

Abstract

The Norwegian Public Roads Administration (NPRA) are investigating the impact of side winds on vehicles travelling over a floating bridge that they wish to construct to shorten travel time. To mitigate the movement of the floating bridge due to high crosswinds, the bridge will be designed in a way that it does not obstruct the wind as much; resulting in high wind impacts on the commuting vehicles. The tractor-trailer combination is a large bluff body and experiences large side wind forces. Due to these forces, it may affect its lateral stability and might result in rollover at high crosswind speeds. This automotive engineering project aims to investigate the forces and moments acting on the truck during strong side winds and design a generic modular model for research use in the road vehicle aerodynamics course. The force investigations were performed numerically using STAR-CCM+ and experimentally through the closed-loop wind tunnel test facility at the Chalmers University of Technology.

SOLIDWORKS was used to design a simplified model of a truck that can be used for research purposes. To accommodate the option of add-ons and to increase the ease of add-ons interchangeability during the wind tunnel testing, the truck design was made modular. The customization could be, for example, the addition of roof fairing, boat tailing or even an American-nose. The down-scaled model was printed and then sanded down and spray-painted for a smoother surface finish and better aesthetics. Assembly of the parts was done using epoxy, super glue and magnets. This model was tested in the wind tunnel, where a sweeping study was performed at a constant wind speed of 30 m/s for varying yaw angles between 0° and 90°. The modular design made it easy to test different configurations, such as different gap sizes between tractor and trailer, and the addition of a roof fairing.

Multiple computational fluid dynamics (CFD) simulations were performed on the 1:1 model to mimic open road conditions and cross-validate the wind tunnel test. STAR-CCM+ software was used to mesh, analyze and post-process the CFD data. A steady-state approach and the k-e turbulence model were used to solve the Reynolds-Averaged Navier-Stokes (RANS) equations. A mesh independence study was performed to ensure the validity of the mesh used for the sweep study. The sweep study tested different relative wind directions between 0° and 90° for the same domain and mesh. A simulation is said to have converged when the force coefficients averaged over 750 iterations lie within 2 drag counts for 750 iterations. A comparison between the CFD and wind tunnel results validate the results as the forces and moments acting on the models follow a similar trend for varying yaw angles. The slight discrepancies in the comparison occurred due to the absence of a moving ground, varying boundary conditions and the mounting struts that act as a flow obstruction.

Keywords: Side-wind, Drag, Yaw, Side-force, Wind tunnel, CFD (computational fluid dynamics), Turbulence, 3D-Printing, CAD (computer aided design)

Acknowledgements

We would like to acknowledge the support provided by our project supervisor Alexey Vdovin with various subjects during the entire duration of the project. We also would like to extend our gratitude to Isak Jonsson for helping us with the 3D printing questions early on.

Finally, we greatly appreciate the assistance and valuable input provided by our examiner Simone Sebben during the entire course of this project to guide us in the right direction.

Contents

List of Figures

List of Tables

1
Introduction

1.1 Background

Side winds play a major role when vehicles are passing over exposed road sections such as floating bridges. Vehicles such as trucks and buses are affected the most, due to their large exposed side areas. This is particularly of interest for floating bridges, as in many cases there are limited other obstacles surrounding the bridges, such as trees or buildings, to limit the impact of side winds. For this reason The Norwegian Public Roads Administration (NPRA) is interested in finding out the impact of strong side winds on vehicles moving over floating bridges.

Vehicles having large side areas are susceptible for rollover and lateral instability when exposed to strong side wind forces. There have been quite a few discussions on commuting over floating bridges when there are predictions of strong winds. Strong side winds could require a bridge to be closed or vehicles would have to travel at lower speeds. Hence, there is the need for an investigation of the resulting forces from side winds acting on a truck model.

1.2 Aim

The aim of this project is to:

- Develop a CAD model of a truck in a CAD software.
- Perform CFD simulations in STAR-CCM+ software on truck model with varying yaw angles.
- A 3D down-scaled (1:18) truck model is printed for wind tunnel testing.
- Interchangeable parts are designed and printed for modularity and for future research purpose.
- Attaining the data of CFD simulations and wind tunnel test results.

1.3 Project Outline

To reach the previously mentioned aims of the project, it is important to define a proper outline of the main objectives to be completed during throughout the project. The used project workflow is shown in Figure 1.1.

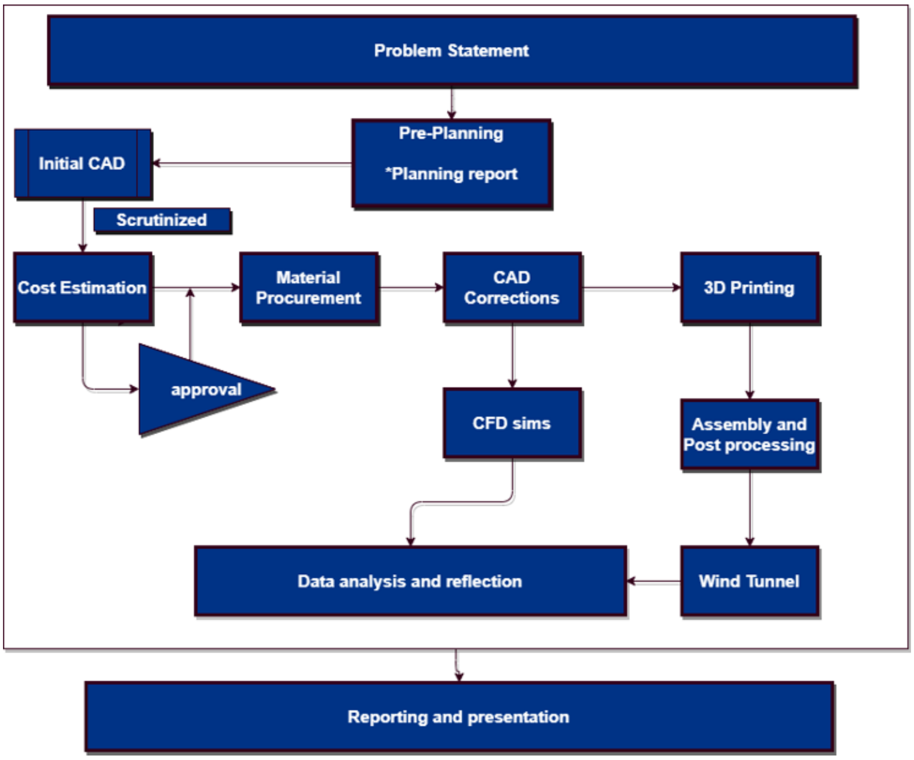

Figure 1.1: Project workflow

1.4 Report Outline

Firstly, a literature study is done in Chapter 2 to have a solid understanding of the subject and the research already performed in the field. Following, the design of the scaled truck model is shown. This includes the design of the CAD model and an explanation of how the model is printed and constructed. In Chapter 4 the setup of the CFD analysis is set out, this includes aspects such as the computational domain, meshing and the turbulence model used. The methods for the wind-tunnel testing of the scaled model are discussed in Chapter 5. Chapter 6 contains the results from both the CFD analysis and the wind-tunnel testing. The results of the study are then discussed in Chapter 7. Lastly, the main points from the discussion and any recommendations are stated in Chapter 8.

2

Literature Study

Various experimental studies have been performed to investigate the cross-wind stability of trucks and busses. Torlund (1999) [3] studied the aerodynamic coefficient around a model bus with side wind yaw angles ranging from -95° to +95°. A yaw angle of 30° was found to be critical, where the lift force and the yaw moment coefficients were maximum. At angles, more than 30° the side force and moment coefficients were found to no be sensitive to change of yaw angle any more.

Certain aerodynamic modifications to a truck can be made to improve the handling stability of a truck under side wind conditions. Zhang et al. (2020) [6] looked at the effect of adding a roof deflector to a tractor semi-trailer on handling stability when crosswinds are present. They found a maximum decrease in lateral acceleration and yaw rate of 14.6% and 16.5% respectively. This shows that certain modifications to the aerodynamic design of trucks can be made to improve their crosswind stability.

An investigation performed on how various parameters affect directional stability of the bus model noticed that the sharp-edged box shape leads to negative pressure acting at the front end, by converting sharp edges to radiused edges reduced the peak values (Juhlin & Eriksson, 2004) [2]. From the analysis results, weight distribution contributed to the largest effect on directional deviation measure. An important aspect to consider while designing a vehicle for low directional deviation is yaw moment overshoot at gust entry when the vehicle exposed to strong winds.

Bettle et al. (2002) [1] examined the relationship between truck speed, wind speed and rollover possibility. From the analysis it was found that when the truck is moving in the windward direction at low speed say around 40 km/h it experienced 120 kNm of force and during $120km/h$ speed of truck it experienced 217 kNm. While that on the leeward lane the truck considerably experienced lesser forces i.e. 82 kNm and 154 kNm for low and high speed of the truck. During crosswind, the magnitude of relative velocity is increased between the truck and the air, in the end resulting drag force will be greater and in the direction of truck's movement the components will be acting both parallel and normal. Lift force is very crucial for drivability as it creates a moment about the longitudinal axis of the vehicle hence reducing the wheel loading on the windward side.

3

Truck Model

This Chapter outlines the design process of the truck model as well as the realization of a physical model. Firstly, the designing of the CAD model in described in Section 3.1. An important aim of the project was to provide a modular model, this aspect explained in Section 3.2. Lastly, in Section 3.3 the process of realizing a physical model from start to finish is set out.

3.1 CAD Model

The truck was modelled based on a generic truck 3D model. Necessary simplifications were made to avoid complicated 3D printing procedures. The simplifications also help in reducing the 3D print times drastically. The base of the truck was kept flat, apart from two fins, on which the wheel housing is supported. The truck was designed in a way to give a generic truck model, complex features like headlamps, heat-exchanger grill and similar items were omitted in the process. The figure below represents the overall truck dimensions in *mm*.

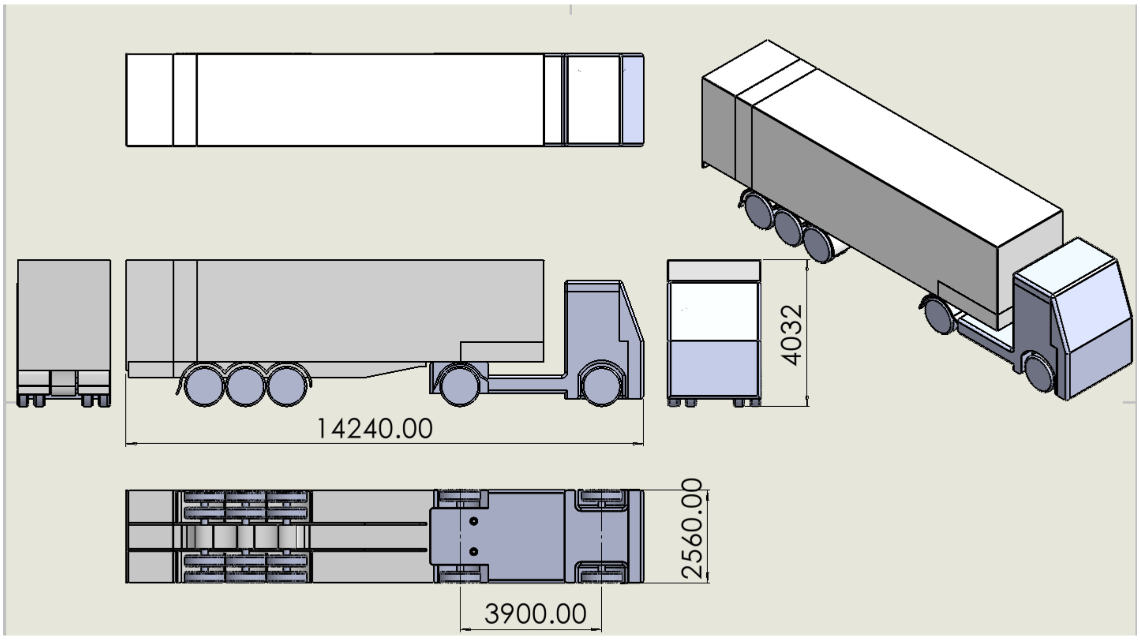

Figure 3.1: All truck views (dimensions in 'mm')

The overall dimensions of the truck are shown in Table 3.1.

Table 3.1: Full size truck dimensions

Dimension	Value [m]
Total length of the truck	14.2
Wheel base tractor	3.9
Track width	2.56
Truck height	4.03

3.2 Modularity of the Model

To make the model more versatile, it was made modular. This also helps in reducing the complexity of the 3D print process. In future iterations of CFD and wind tunnel testing, changes can be made with respect to the roof such as adding a roof fairing or replacing the European nose with an American nose. Figure 3.2 represents the modularity of the tractor. Similarly, the trailer is divided into two parts, so that the rear end can be replaced with different configurations, such as a boat tail. In Figure 3.3 the modular parts of the trailer are shown.

The model add-ons that were designed, was only a roof-fairing, shown in Figure 3.2. As far as the boat tail is concerned, different designs were proposed, but due to lack of time they were not evaluated in CFD to determine which design would be beneficial and thus no such model was manufactured.

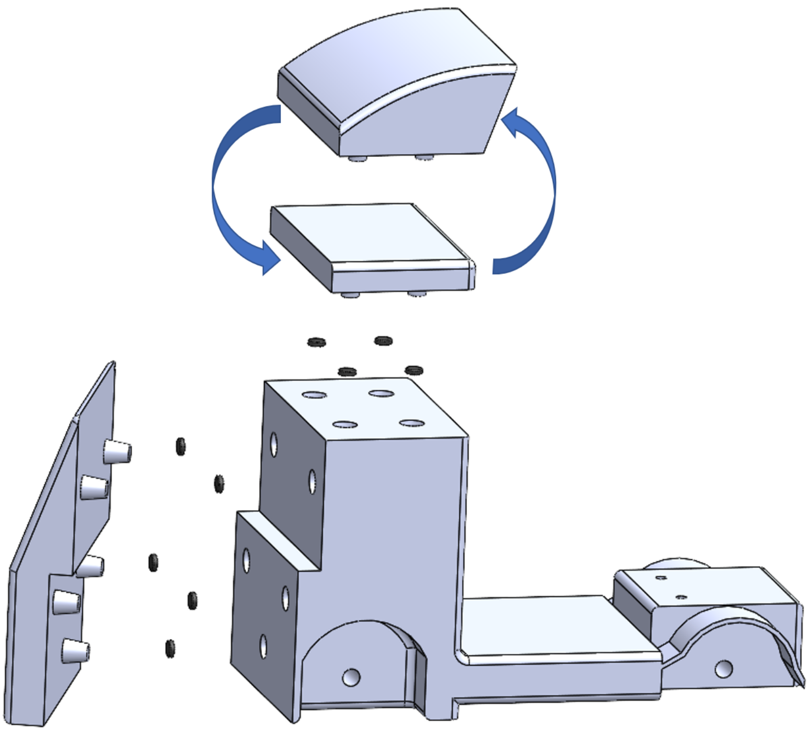

Figure 3.2: Modularity of the tractor

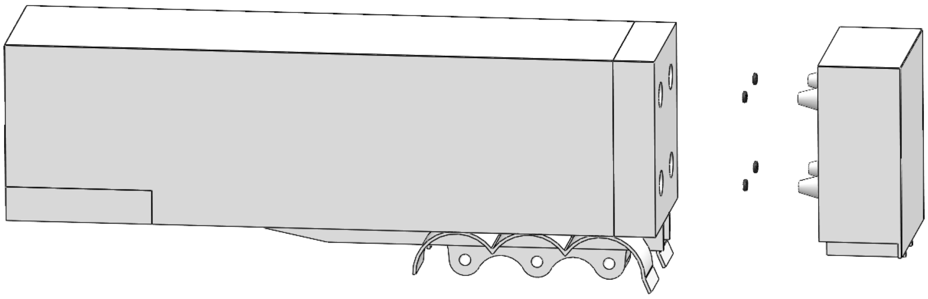

Figure 3.3: Modularity of the trailer

3.3 Physical Model

This section includes the process of realizing a physical model. Firstly, in Section 3.3.1 the down scaling of the full size model to the scaled model used in the wind tunnel is explained. After which, the manufacturing process is described in Section 3.3.2. Section 3.3.3 outlines the assembly of the manufactured parts. Lastly, the finishing and painting of the model is described.

3.3.1 Scaling of the Model

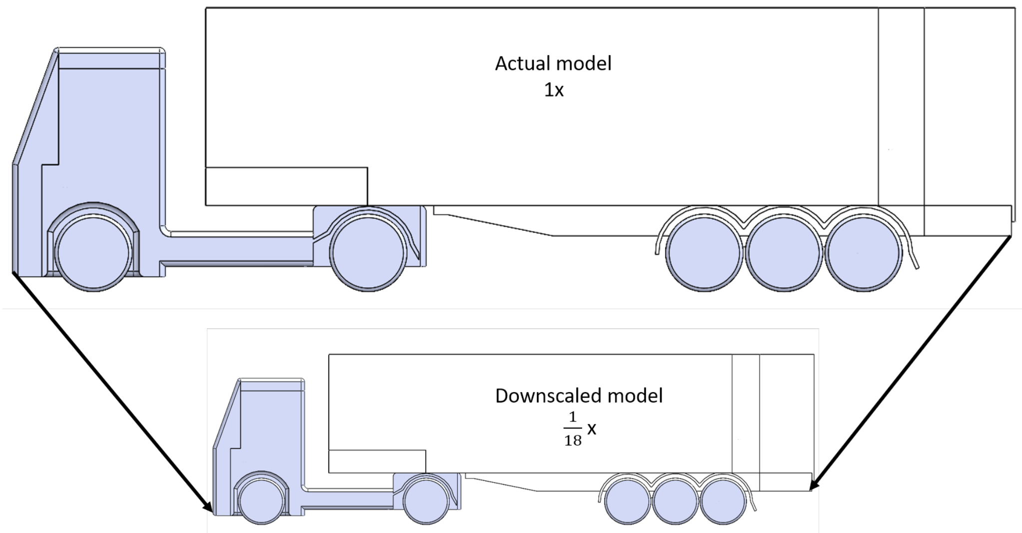

Figure 3.4: Down-scaling of the truck

The truck model was downsized to 1/18$^{\text{th}}$ (as shown in Figure 3.4) of its original size. The scaling factor was chosen in a way to avoid blockage effects in the wind tunnel and print-ability of the model. The scaling factor also decided where the centre of mass would lie on the wind tunnel scale. The design was based on previous year's mounting plate for the bus model. Keeping the truck almost centred on the mounting plate is vital to avoid imbalance and unnecessary movements of the truck at high yaw winds. Based on the measurements of the mounting plate and wind tunnel dimensions, the model was downsized to the above mentioned scaling factor.

3.3.2 Manufacturing Process

As mentioned in Section 3.2, the truck model to be used in the wind tunnel experiments was designed modularly to enable testing of different configurations. Two different 3D printers were used to build the components of the truck, an industrial one for the bigger part, namely the main part of the trailer, and a commercial one for the remaining parts, in order to get a detailed and smoother print. More specifically, due to restrictions of the commercial 3D printer size to produce the physical model, both the tractor and the trailer were split. The bulk part of the trailer was divided into the main part, the underbody fins, the wheel housing and the bottom and back parts that include holes (Figure 3.5) and the tractor was separated into two parts, namely the main part and the tractor/trailer connector (Figure 3.6).

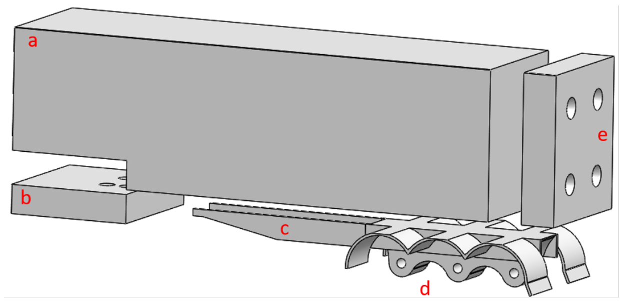

Figure 3.5: Trailer split into: *a*: Main part, *b*: Bottom part with holes, *c*: Fins, *d*: Wheel housing, *e*: Back part with holes

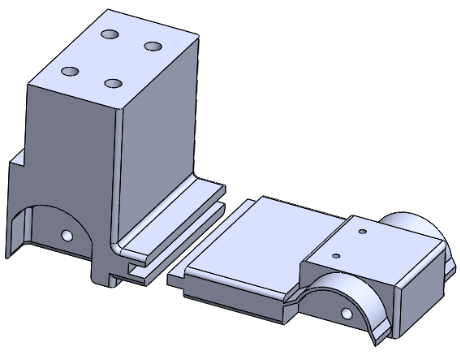

Figure 3.6: Tractor split into: *Left:* Main part, *Right:* Tractor/trailer connector

Both of the aforementioned 3D printers utilize the Fused Deposition Modelling (FDM) technology, and the material used was PLA (Poly-Lactic Acid). Compared to other technologies, FDM is low-cost but with lower dimensional accuracy and resolution[1].

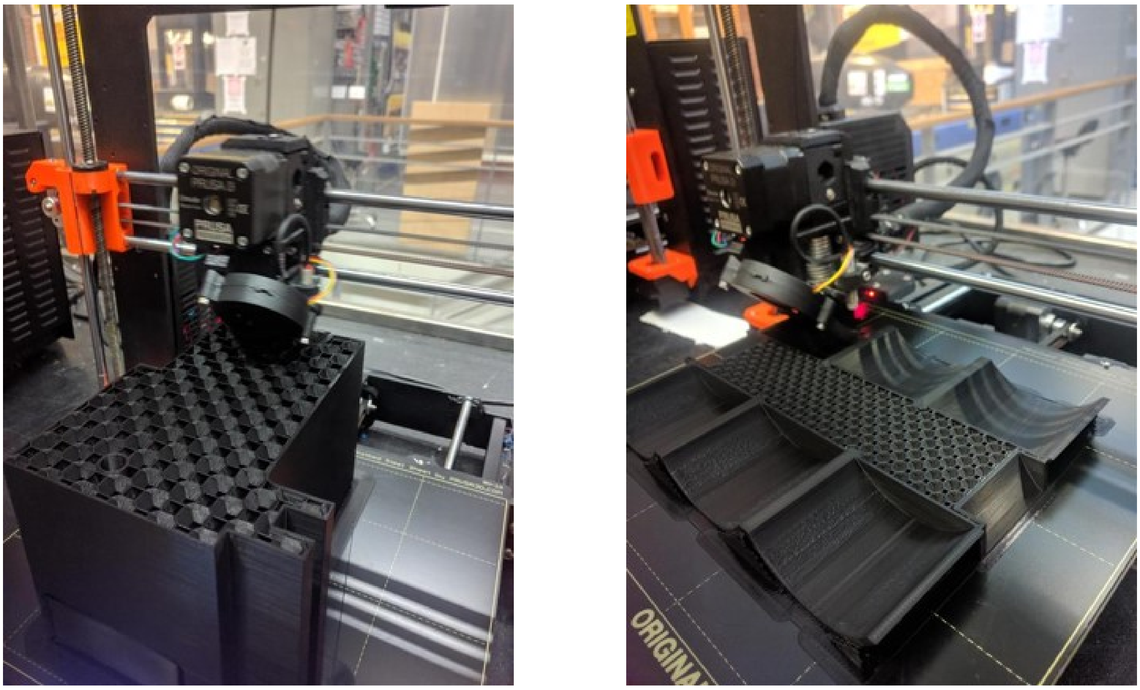

(a) Main tractor part

(b) Trailer under body including wheel covers

Figure 3.7: 3D printing process in Prusa MK3S with a 3D-honeycomb infill pattern

One of the most common weaknesses of this technology is warping. Warping is caused by the different cooling rates of different regions of the printed model. When the material is cooled and solidified with different rates, internal stresses are building up, which in turn cause the underlying layer to be pulled upwards (to warp) [1]. Using PLA, the warping problem is less likely to happen compared to other materials, and, also, rounded corners, such as fillets, can help to prevent this problem. Another problematic area of the FDM is the visible layer lines, which require post-processing and surface treatment of the model [1].

However, since the truck model does not have any complex details, the accuracy of the printing does not have to be very high and additionally, the cost of the post-processing is lower compared to using more complex 3D printing methods. Consequently, the cost efficiency and availability of the FDM overshadows its drawbacks, and thus it was selected as the desired method of 3D printing.

As far as the material used is concerned, PLA is a thermoplastic material that is commonly used in 3D printing. PLA has the very good visual quality and due to its low printing temperature is less likely to warp, which is important when printing big parts, which are more prone to warping. Moreover, its adhesion ability is very high.

[1] https://www.3dhubs.com/knowledge-base/introduction-fdm-3d-printing/#what

However, its tensile strength is low and PLA models are quite stiff and thus brittle[2]. Nevertheless, the drawbacks of using PLA do not influence the quality of the truck model regarding the wind-tunnel testing, since its manufacturing does not require processes that are affected by the PLA mechanical properties and the experiment type and conditions make the PLA an acceptable model material.

Different parameters during the printing process lead to different model quality and characteristics. In order to compromise between a light-weighted and strong structure, parameters like infill density and infill pattern had to be tweaked to get the desired result. The wall thickness was kept at 3 mm, by defining the number of layers of the perimeters, and the infill density was chosen as 5%, leading to a light but strong enough model. It is noted that the wheels, which were used to mount the truck when tested in the wind tunnel, were designed with 100% infill to be able to carry the weight of the model, while attached on the mounting struts.

The printer used for the smaller parts of the truck was a Prusa MK3S. This particular printer has a removable heatbed, consisted of a spring steel sheet with PEI (Polyetherimide) surface [3]. The PEI coating is important for the print adhesion and it enables an easier printing process with minimum clean-up effort by excluding the need to use tape or glue sticks, to achieve good adhesion quality. The final specifications of the printing process and its duration are presented in Table 3.2.

Table 3.2: Specifications of printing process

Property	**Value/Particulars**
Filament material	PLA
Infill	5%
Infill pattern	3D Honeycomb
Layer height	0.1 mm
Solid surface layers (top & bottom)	20
Total printing time (approximately)	**65 hrs**

3.3.3 Assembly

After all the parts of the model are printed, they were assembled using magnets, super glue and screws. More specifically, the modular parts, which include the roof fairing and the face of the truck, as well as the rear end of the trailer, were attached to the model with neodymium magnets. These are strong enough to hold them (each has an adhesive force of 0.9 kg) in place during the experiments, while they enable easy attachment/detachment. The trailer consists of four parts, excluding the rear end (as shown in Figure 3.3), which were glued together.

The only parts that were not printed were the axles, to ensure their robustness and avoid breaking. Thus, the material which was used is steel. The axles were then

[2] `https://amfg.ai/2018/07/02/pla-3d-printing-all-you-need-to-know/`
[3] `https://www.prusa3d.com/original-prusa-i3-mk3/`

glued to the holes of the truck body and the wheels.

The trailer and tractor were connected using M6 screws. To avoid threading of the trailer, the model was printed with holes to which threaded inserts were glued and the space surrounding the inserts was filled with plastic filler. Two different sets of holes were designed on the trailer to give the ability to change the gap between the tractor and the trailer.

3.3.4 Finishing & Painting

In order to ensure that the printed parts have the same surface quality when tested in the wind tunnel, a surface treatment was necessary. The 3D printing method produces components with irregular surfaces, due to the visible layer lines. These irregularities were first sanded down with different sandpapers and then a spray filler for plastics was applied. As soon as the spray filler was dried and hardened, it was sanded down again so that only the required filler remained, producing a homogenous and smooth surface all over the components (Figure 3.8a).

Following the spray filling step, the spray paint was applied on the components. The painting was essential so that the skin friction coefficient would resemble an actual truck surface (Firgure 3.8b). The color of the paint was chosen black to give a nice look to the truck and also facilitate the visualization of the white tufts' motion, which are used in the wind tunnel experiments.

(a) Spray filler is applied for a smooth finish

(b) Black spray paint is used as a finish

Figure 3.8: Finishing of the tractor part

When the surface treatment was finished the model was assembled, as shown in Figure 3.9. Figure 3.10 shows the assembled model with the designed roof fairing.

Figure 3.9: Finished product - base model

Figure 3.10: Finished product - base model with roof fairing

4
CFD Model

This chapter outlines the approach to the CFD analysis performed on the CAD model of the truck as shown in Chapter 3. The model is meshed, analyzed and post processed using STAR-CCM+. Multiple CFD simulations were performed on the 1:1 model to simulate open road conditions. The coordinate system and the non-dimensional coefficients used for the simulations are described in Section 4.1 to better understand the further sections. Defining the computational domain (Section 4.2) is important to make the simulation more efficient, as a larger domain may increase computational cost and a smaller domain may not resolve the disturbances in the flow. Selecting appropriate meshing models and parameters are key to a successful simulation. This alongside the mesh independence study is described in Section 4.3 while Section 4.4 states the simulation parameters. The convergence criteria for the ensuring successful simulations are defined in Section 4.5.

4.1 Coordinate System & Non-dimensional Coefficients

The user coordinate system is shown in Figure 4.1. Positive X-direction lies along the length of the truck towards the rear. The right side of the truck is positive Y-direction and the truck height points in the positive Z-direction. The force in the X-direction is referred to as drag, the force in the Y-direction as side force and in the Z-direction as the lift. The moments about these axes will be referred to a roll, pitch and yaw around the x, y and z-axis respectively.

(a) Side view **(b)** Rear view

Figure 4.1: Defined coordinate system

The equations for the coefficients of forces and moments are given by equations 4.1 to 4.6.

$$C_D = \frac{2 * F_x}{\rho * v^2 * A} \quad (4.1)$$

$$C_{m_x} = \frac{2 * M_x}{\rho * v^2 * A * L} \quad (4.4)$$

$$C_S = \frac{2 * F_y}{\rho * v^2 * A} \quad (4.2)$$

$$C_{m_y} = \frac{2 * M_y}{\rho * v^2 * A * L} \quad (4.5)$$

$$C_L = \frac{2 * F_z}{\rho * v^2 * A} \quad (4.3)$$

$$C_{m_z} = \frac{2 * M_z}{\rho * v^2 * A * L} \quad (4.6)$$

The nomenclatures ρ denotes density of air at 25 °C i.e. 1.184 kg/m^3, v denotes velocity (25 m/s), A denotes frontal area of the truck (10.01 m^2), L denotes total truck length (14.2 m). F_x. F_y and F_z are the aforementioned forces, while M_x, M_y and M_z are the aforementioned moments.

4.2 Computational Domain

A paper investigating crosswinds on-road vehicles by Youhanna E. William [5] mentions the best practices for domain size to be such that the length of the domain should be 14.74 times the vehicle length, the width must be 37.9 times the vehicle width, and the height must be 12.14 times the vehicle height. The maximum truck dimensions are $14.2 * 2.56 * 4.03$ m. Using the approach mentioned in the paper results in a domain that is 213 m in length, 98 m in width and 51 m in height. In the X-axis, the truck is placed inside this domain such that it leaves 4 truck lengths in front of it and 10 truck lengths in the wake region. Along the Y-axis, the truck is placed at 40% domain width from the left side inlet wall, leaving 60% of the width to resolve the side-wake region. The truck is placed onto the road such that the wheels exceed the domain by 10 mm in the negative Z-direction[1]. This is done to accommodate tyre compression during driving conditions in a computationally affordable manner.

[1] Landi, S., Drive your vehicle aero! Part I - Tips and tricks for steady-state simulations, *Simcenter TV Broadcast*

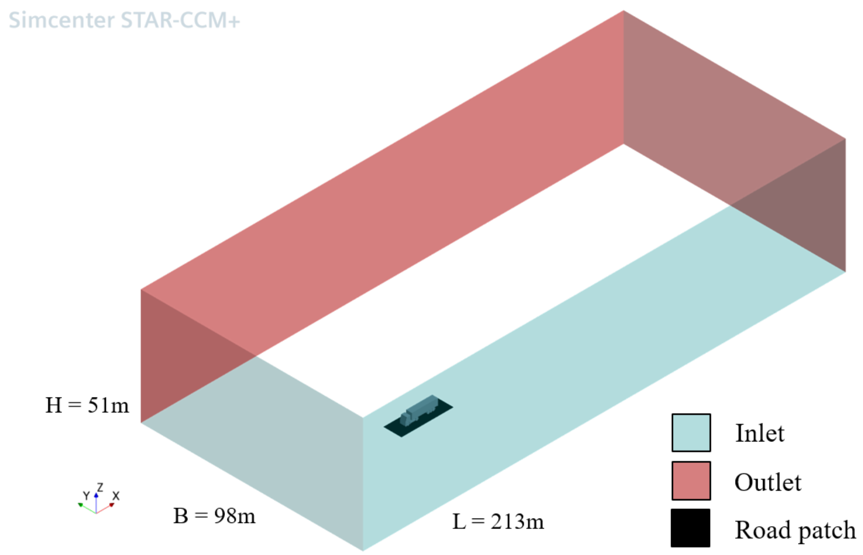

Figure 4.2: Computational domain

4.3 Meshing

As the truck was modelled in SOLIDWORKS as an assembly, Surface Wrap operation was performed on it to get the model ready for the simulation. The target size for the wrapping cell was set to 0.01 m with a finer mesh for curvatures and corners. This being a surface preparation operation, it had a finer mesh which is remeshed in further operations. This surface wrapped model was subtracted from the computational domain to create the region of air flow. The meshing of the region was performed using an automated part based meshing operation. The meshing models used were Automatic Surface Repair, Surface Remesher, Polyhedral Mesher and Prism Layer Mesher. The former two are surface operations while the latter two are volume operations.

4.3.1 Surface Mesh

Surface Remesher was used to define the surface mesh of the entire region. The aim was to have a large cell size near the boundaries of the domain and smaller cells around the truck to reduce computational cost without affecting the accuracy of the simulation. To achieve this, refinement regions were defined around the truck including the wake regions and a slow surface growth rate produces a smooth transition wherever the cell size increments. The refined surface mesh around the wheels can be seen in Figure 4.3. Smaller cell sizes were needed to capture the curvatures around the wheels and housings. Automatic Surface Repair, as the name suggests, repairs the generated surface mesh by either ignoring or modifying a feature edge when the face quality value falls below a specified threshold value.

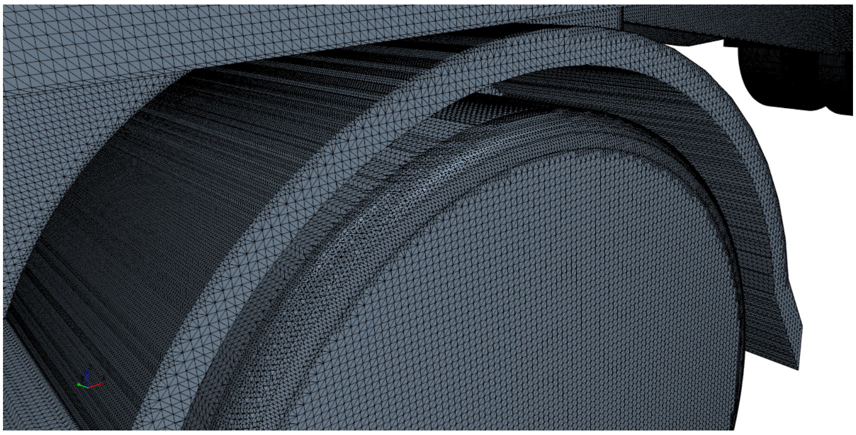

Figure 4.3: Surface mesh near the tractor wheel

4.3.2 Volume Mesh

Polyhedral mesh is a widely used volumetric meshing model. Its versatility for complex flows and large wake regions is suitable for this case. The polyhedral cells are set to be very large at the extremities of the domain, and are refined near the truck as seen in Figures 4.4 and 4.5. The refinement regions were updated after a few simulations to resolve the wakes efficiently.

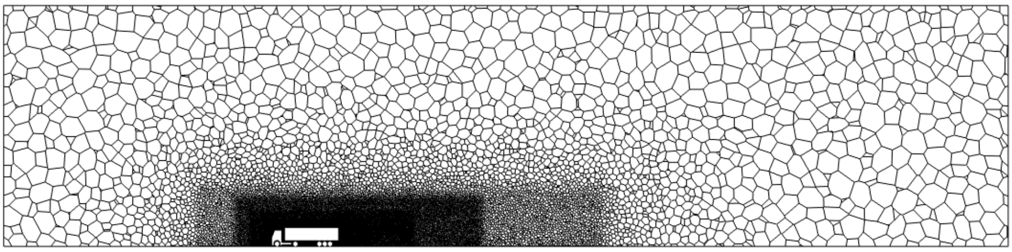

(a) Side view at Y = 38.2 m (left edge of the truck)

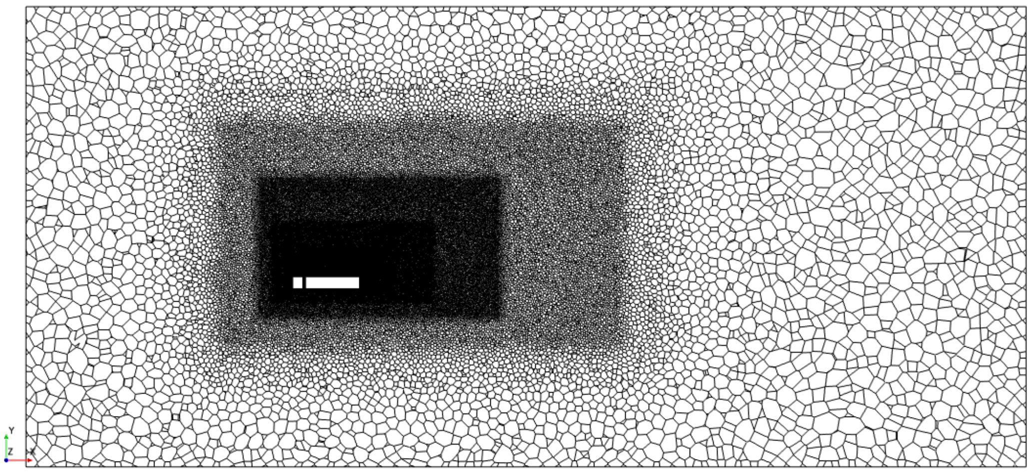

(b) Top view at Z = 1.8 m

Figure 4.4: Volume meshes in the complete domain

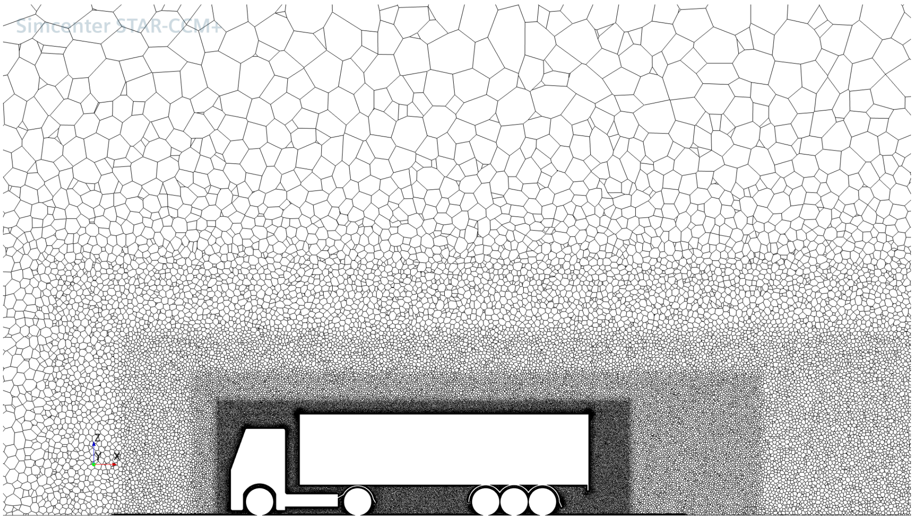

Figure 4.5: Mesh around the truck at Y = 38.2 m (left edge of the truck)

The prism layer mesher is used to capture the boundary layer formation over the body; in this case, the truck and the road patch (more about the road patch in Section 4.4). The prism cells are defined such that first the cell on the body has a desired y^+ value ranging between 30 - 300 for the 'All y^+ Wall Treatment' model (Section 4.4). Wall y^+ is a non-dimensional distance used in turbulence modelling. It is defined as:

$$y^+ = \frac{y * u_T}{\nu} \tag{4.7}$$

Where, y is the first cell thickness, u_T is the friction velocity and ν is the kinematic viscosity of the fluid. After some initial simulations, it was decided to keep six prism cells such that the first cell has a thickness of 0.005 m and the final prism cell has a thickness of 0.022 m. The final prism thickness and total layers were decided based of the surrounding polyhedral mesh of 0.035 m in size. The prisms layers can be seen in Figure 4.6 while the resultant y^+ values for the simulation can be seen in Figure 4.7. The large stagnation areas and sharp corners result in extreme values on both sides of the spectrum and require extra computational effort in terms of local refinements.

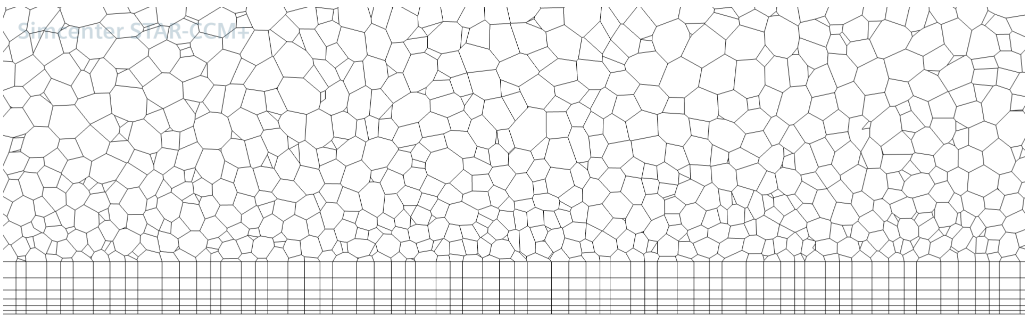

Figure 4.6: Prism cells over the trailer

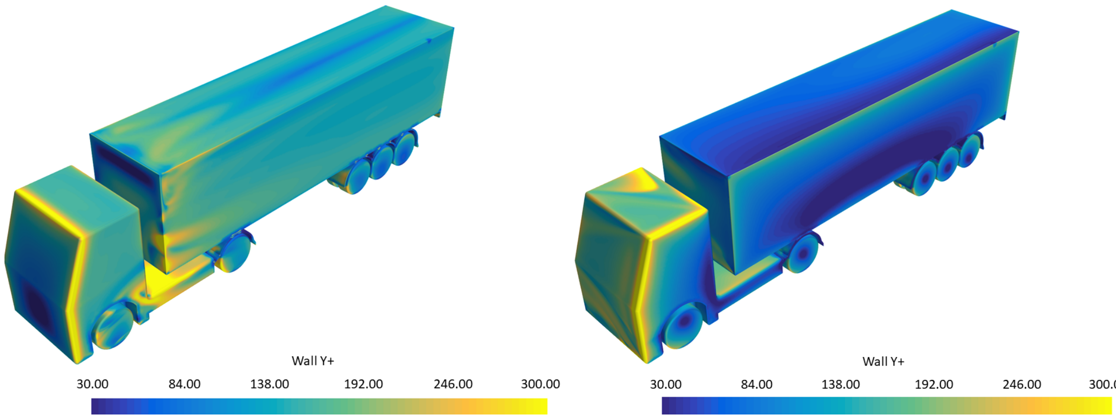

(a) 0° yaw **(b)** 90° yaw

Figure 4.7: Wall y$^+$

4.3.3 Mesh Independence Study

The purpose of this study is to ensure that the simulation result does not depend over the mesh cell count and to find a mesh that provides reliable results without being computationally expensive. Several meshes were generated ranging from 37 million cells to 63 million cells. Each mesh was simulated for 0° yaw and 90° yaw condition, where the drag and side force coefficients were monitored respectively. From Figure 4.8, it is noticed that refinement of the mesh does not vary the C_D much, while the C_S does vary but change in value is very less. Thus, the 44 million mesh case was judged to be the optimal choice for this study.

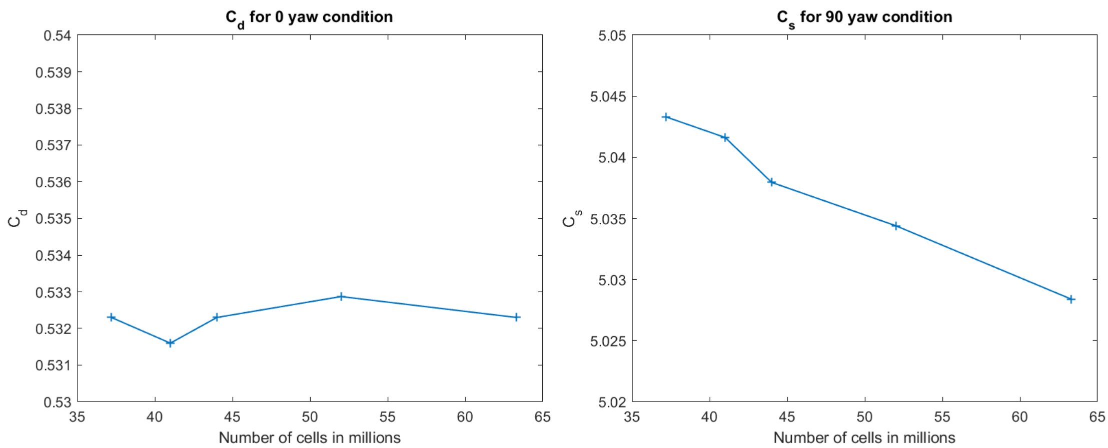

(a) Drag force coefficient for 0° yaw **(b)** Side force coefficient for 90° yaw

Figure 4.8: Force coefficients vs number of mesh cells

4.4 Simulation Parameters

To perform the CFD sweep on the truck, boundary conditions need to be defined and physics models must be chosen.

The boundary conditions are as follows:

- **Inlet:** Magnitude of 25 m/s varying in direction between 0° - 90° (as shown in Figure 4.9).
- **Road:** split into two sections. The road patch around the truck, sized $22m$*$8m$, to portray a moving road with a no-slip condition. The rest of the road has a slip condition to avoid development of the boundary layer. This is seen in Figure 4.2. The patch has a fixed velocity of 25 m/s in the positive X direction, i.e. opposite to the truck movement.
- **Roof:** Symmetry plane.
- **Outlet:** Pressure outlets.
- **Wheels:** Local rotation rate (45.46 rad/s) is provided based off the truck speed and wheel diameter.

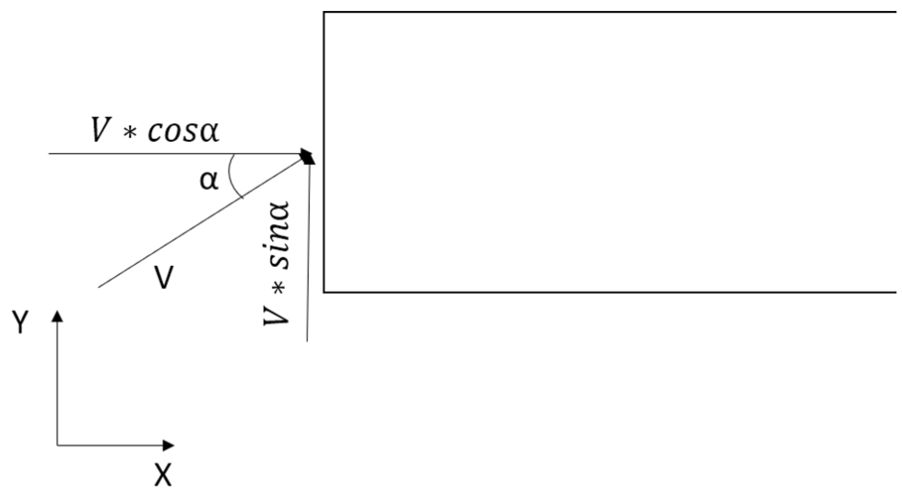

Figure 4.9: Relative velocity implementation

The physics models chosen are as follows:

- **RANS solver:** Reynolds-Averaged Navier Stokes solver was used for this simulation. Detached/Large eddy simulations could prove to be slightly more accurate for this case, but have extremely high computational requirements. Thus, RANS solver was selected.
- **Incompressible flow:** As the fluid velocity does not exceed Mach 0.3, constant density is assumed.
- **Steady flow:** The flow is assumed to be steady for this simulation.
- **k-ϵ turbulence model:** the k-ϵ turbulence model is selected for its robustness

to resolve far field flow.

- **All y^+ Wall Treatment:** Selected for it's robustness. The goal was to keep the y^+ values between 30 and 300, which is high wall treatment. But given the large stagnation regions, the y^+ values drop below 30 at some places.
- **Coupled flow:** Selected to avail Grid Sequence Initialising which helps to converge the solution faster.

4.5 Convergence Criteria

The criteria set to declare a solution as converged was that the force coefficients averaged over 750 iterations should lie within two counts for 750 iterations. The graphs can be seen in Figure 4.10, for a specific angle. Averaging was needed especially for higher yaw angles where the extreme wakes with large vortices had greater fluctuations.

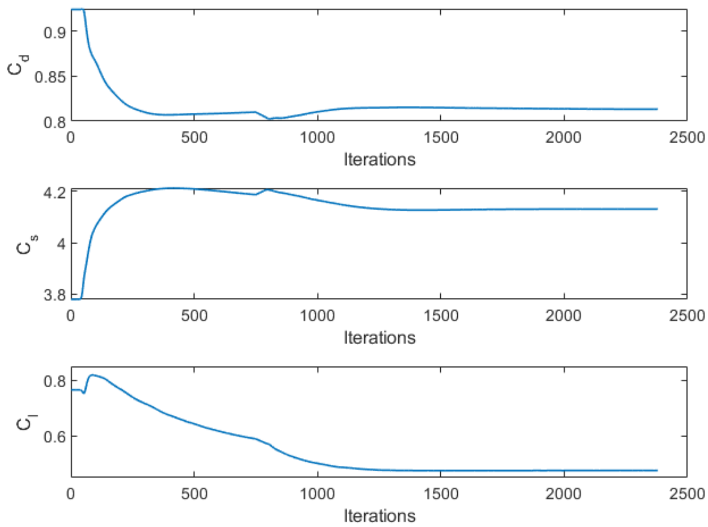

Figure 4.10: Convergence criteria for 45° yaw

To judge the convergence of simulation several aspects should be looked at: *residuals*, *monitoring of engineering quantities* and *visualizing of the flow field* [2]. Good practise shows that the residuals should drop by three orders of magnitude, and the residuals should flatten out which, indicates that they will not change significantly with further iterations. The maximum velocity in the domain was also observed to verify if there were any irregularities present. A picture of the residuals taken from STAR-CCM+ can be seen in Figure 4.11

[2] `https://support.sw.siemens.com/en-US/product/226870983/knowledge-base/KB000014875_EN_US?pid=sc%3Apc-typeahead&index=content-external&audience=external`

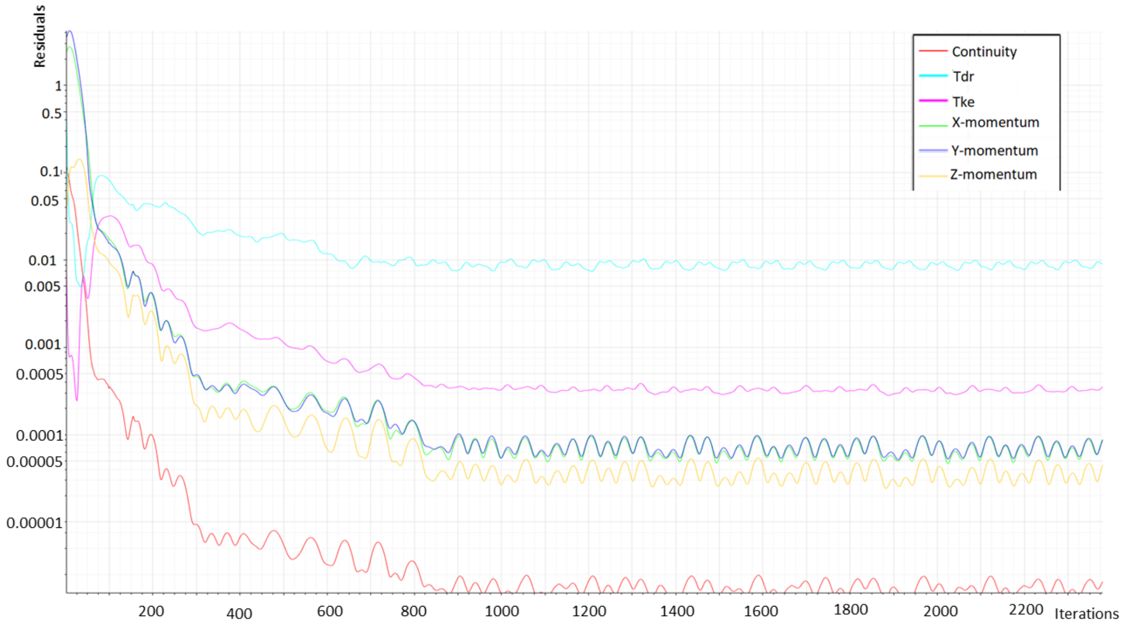

Figure 4.11: Force coefficients convergence graph for the 4° yaw case

5

Wind-Tunnel Testing

The approach to the wind-tunnel testing performed is discussed in this chapter. Firstly, an important aspect to consider is the proper mounting of the model within the wind-tunnel, this is explained in Section 5.1. Section 5.2 outlines the execution of the performed tests in the wind-tunnel. Lastly, it is important to process the obtained data in such a way that the results can be analysed, this is discussed in Section 5.3.

5.1 Mounting in the Wind-Tunnel

The forces and moments acting upon the truck model are measured using a scale. The scale can be rotated along the z-axis which allows the model to be tested at various yaw angles. An important aspect to be considered is that the measured force and moments by the scale should purely come from the air flow interacting with the model. It is therefore important to make sure that the mounting rods do not come into contact with the rotating floor beneath the mode, as this would alter the measured data.

The mounting points on the truck were determined while considering the mounting device that needed to be used. Additionally, they were chosen to ensure that the model was centered in the wind-tunnel when rotated, and thus leaving a large enough gap between the model and the side wall of the test section. Having these two points in mind, the appropriate mounting points were determined to be on the connection between tractor/trailer and on the wheel on the second axle of the trailer, for both the small and the increased gap (Figure 5.1). It should also be noted that the model is mounted in the wind-tunnel such a way that the wheels do not touch the floor of the test section, as this again would alter the measured data.

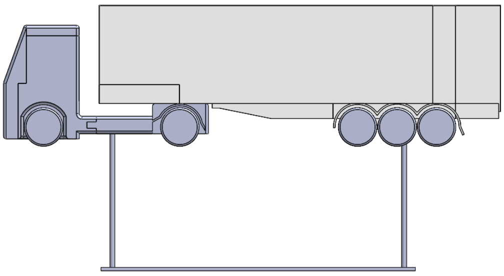

(a) Base model - small gap

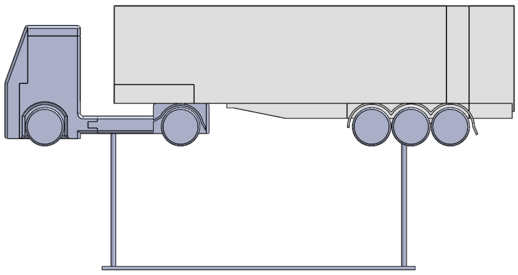

(b) Increased gap

Figure 5.1: Mounting positions

5.2 Test Execution

The main aim of the wind-tunnel testing was a yaw angle sweep which was performed on four different configurations of the scale model. The tested configurations are further described in Section 5.2.1 and the yaw angle sweep is explained in Section 5.2.2. Further flow visualization during testing is discussed in Section 5.2.3.

5.2.1 Configurations Tested

As mentioned previously, the scale model is modular and thus different configurations of the model could be tested. Four different configurations were tested as shown in Figure 5.2. The "base model" configuration has a gap between the tractor and trailer of 30 *mm*, while the "increased gap" configuration has an increased gap of 50 *mm*. The third configuration that was tested, was the base gap size plus a roof fairing. Lastly, the increased gap was tested together with a roof fairing.

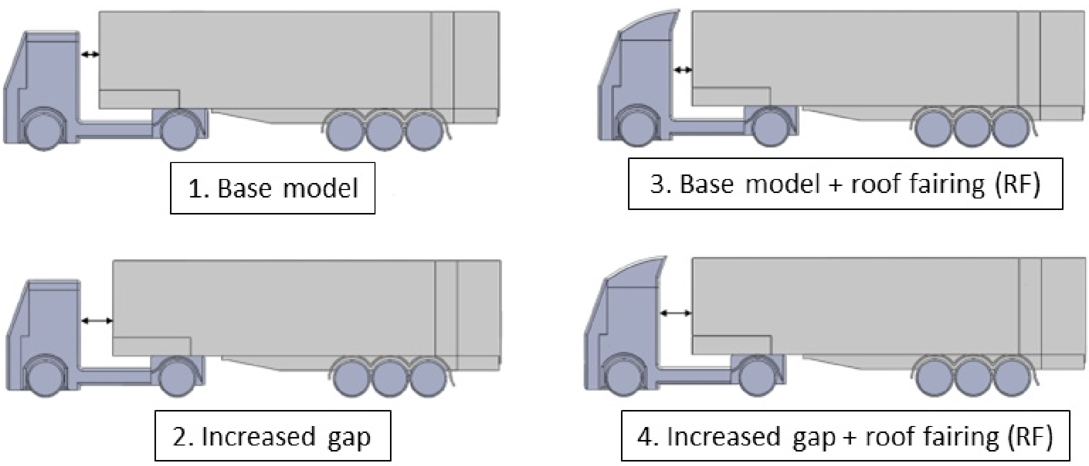

Figure 5.2: Wind-tunnel testing configurations

5.2.2 Yaw Angle Sweep

The main aim of the study was to investigate the sensitivity of a truck model to side winds, thus a yaw angle sweep was performed. A sweep was performed from 0° to 110°, with steps of 3° up to 15° yaw, and steps of 5° from 15° to 110° yaw. This sweep was performed both ways (0° to 110° and 110° to 0°) for confirmation purposes. Before the sweep the model was tested at various airflow velocities to check up to which airspeed the model could safely be tested. This was determined to be 30 m/s and thus this velocity was used for the yaw angle sweep. The following steps were taken while performing the experiment:

1. Zero the wind-tunnel scale at the start of the sweep
2. Set air velocity to 30 m/s
3. Check that the mounting rods are not touching the moving plate
4. Save data when the measurement is stable
5. Change yaw angle
6. Check that the mounting rods are not touching the moving plate
7. Save data when the measurement is stable
8. Repeat

It should be noted that the scale was not zeroed between each change of yaw angle to save time as access to the wind-tunnel was limited. Several measurements at a number of specific angles were performed where the scale was zeroed, in order to determine what effect of not zeroing the scale had on the measurements.

5.2.3 Flow Visualisation

Besides the performed yaw angle sweeps, some flow visualisation was performed using tufts. Tufts were added to several parts of the scaled model, such as the roof fairing or rear of the trailer, to show when flow separation occurred at different yaw angles. Furthermore, with the use of a tuft attached to a rod the behaviour of the flow near different parts of the model could be shown, as well as the how the wake developed behind the model.

5.3 Data Processing

Proper processing of the data is necessary in order to analyse the results of the wind-tunnel testing itself and for being able to compare it with the results from the CFD analysis. The data from the scale is exported to a text file, which was analysed with a MATLAB script.

As all sweeps were performed back and forth outliers in the data, due to for example the mounting rods touching the moving plate, could easily be identified. The function "polyfit" in MATLAB was used to negate small disturbances between the two data measurements.

To calculate the force and moment coefficients from the measured data, equations 4.1 to 4.6 are used. Where F, M, ρ and v are determined from the wind-tunnel testing. The frontal area of the model A is set to 0.0310 m^2 and the model total length L is 0.7889 m.

In order to account for blockage effect due to the model, a correction factor F_{corr} is applied to the measured data, according to equation 5.1 [4]. Where A_{proj} is the projected area of the model in yz-plane (e.g. the area in direction of the flow), which is found for each tested yaw angle using STAR-CCM+. S is the cross-sectional area of the test section (2.25 m^2).

$$F_{corr} = \left(1 - \frac{A_{proj}}{S}\right)^{1.288} \tag{5.1}$$

6
Results & Discussion

This chapter contains the results and discussions from the CFD and wind-tunnel analysis. Section 6.1 discusses and interprets the force and moment coefficients obtained from the CFD sweep study with the help of flow visualisation. A comparison is made between the CFD results and the results obtained from the wind-tunnel testing in Section 6.2 to cross validate the data. Finally, in Section 6.3 the results from the wind-tunnel testing for the four configurations is discussed.

6.1 CFD Results

6.1.1 Flow Visualisation Through CFD

Coefficient of pressure
The coefficient of pressure (C_p) is a dimensionless term that correlates to the forces acting on the body, and is defined as follows;

$$C_p = \frac{p_{stat} - p_{\infty,stat}}{p_{\infty,dyn}} \tag{6.1}$$

where,

- p_{stat} is the static pressure at the point of evaluation
- $p_{\infty,stat}$ is the static pressure in the free stream fluid
- $p_{\infty,dyn}$ is the dynamic pressure in the free stream fluid

The pressure coefficient is an overall vehicle performance parameter and the surface normal needs to be identified to understand the direction of the acting force. By resolving the forces in the three directions namely X, Y and Z, the drag, side and lift force contributions can be visualized respectively. A positive value indicates a pushing force on the surface while a negative value indicates a pulling force in the direction of the surface normal. The Figure 6.1 shows the pressure coefficient for various yaw angles. The shift of the high pressure region can be seen from the front of the truck to the side of the truck for 0° yaw and 90° yaw respectively. An interesting effect is seen in Figure 6.1c, where a low pressure region is generated at the front of the truck. This contributes to the negative drag seen in Figure 6.3.

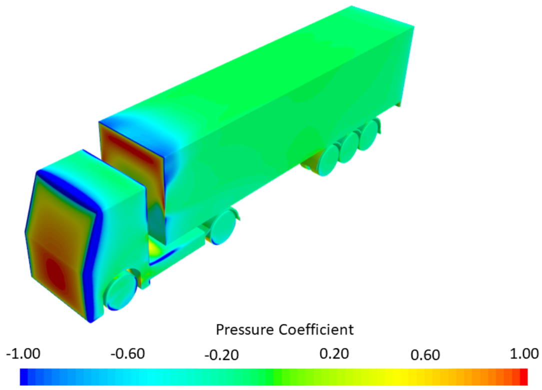

(a) 0° yaw

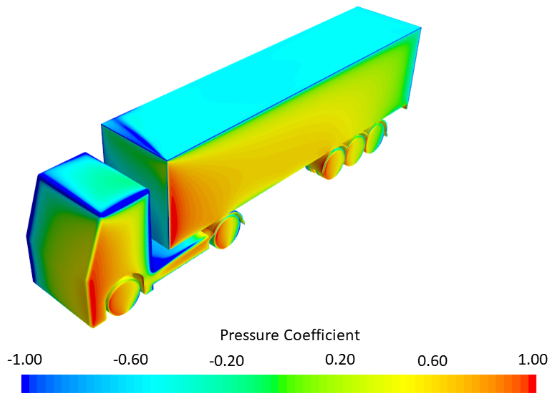

(b) 45° yaw

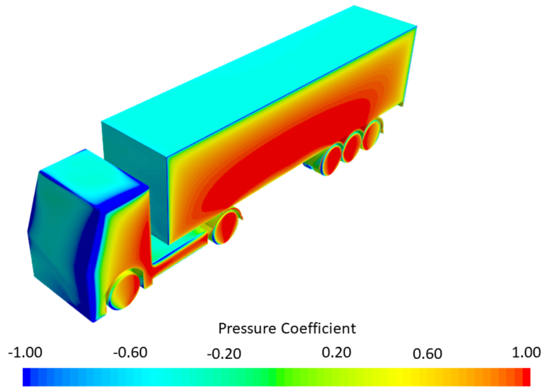

(c) 90° yaw

Figure 6.1: Coefficient of pressure on the truck

Velocity contour

The velocity contours show how the flow propagates when the yaw angle is varied and a few examples are shown in Figure 6.2. The wake regions can be easily identified with the vector contours and as the yaw angle increases, the re-circulation region expands. Velocity contours help visualize the changes in the flow. Consider the 90° yaw case shown in Figure 6.2c. Over the upwind side of the truck (-Y direction), there exists a bright red spot at the front end. This is caused due to the fillet provided on the tractor face which accelerates the flow without causing separation. Thus, pressure reduces over the front end of the tractor. While the sharp edge at the rear end of the trailer causes flow separation and also results in a lower pressure over the rear surface. These pressure coefficients can be seen in Figures 6.4c and 6.4f.

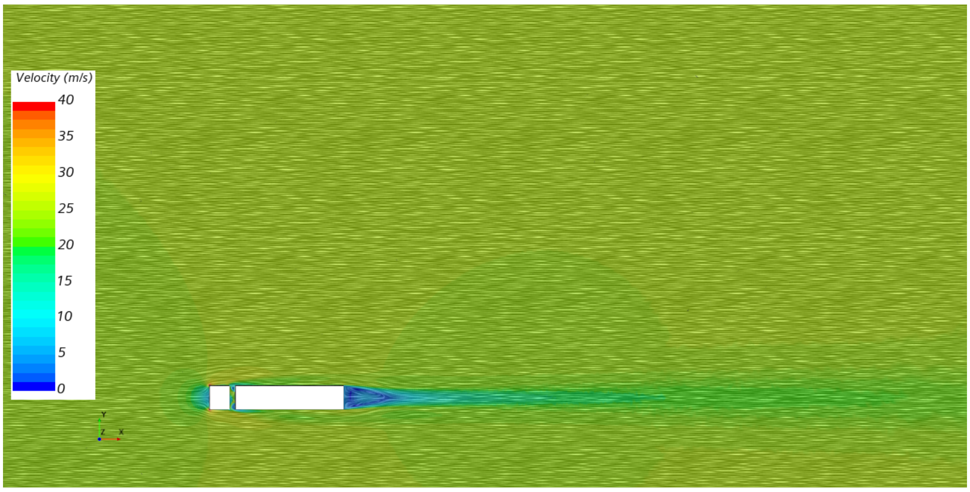

(a) 0° yaw

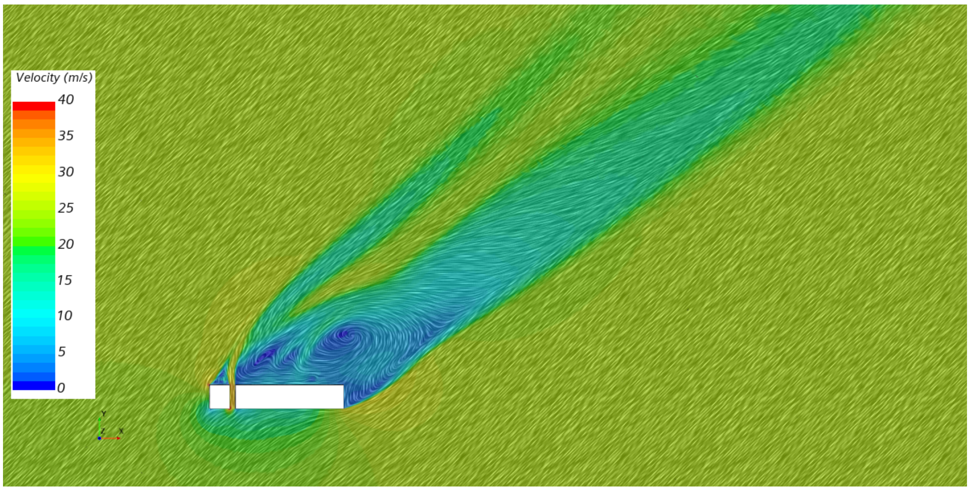

(b) 45° yaw

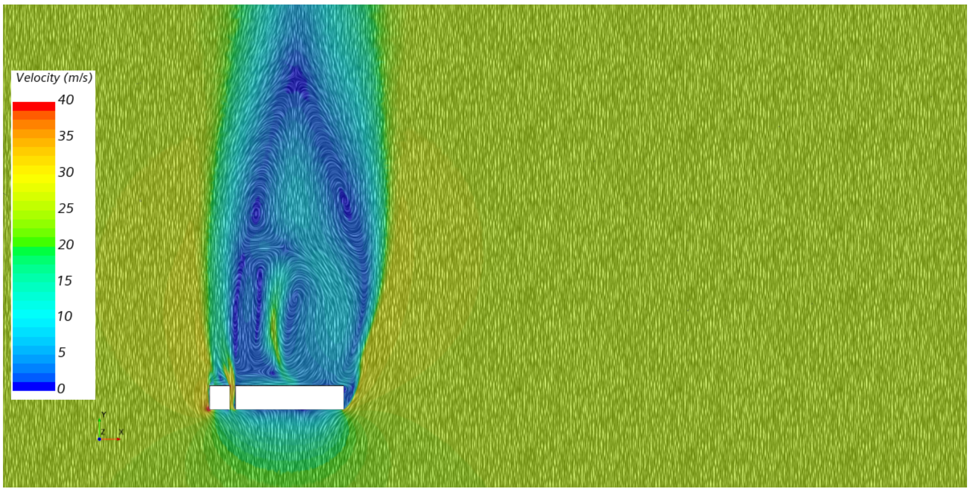

(c) 90° yaw

Figure 6.2: Velocity contours around the truck at Z=1.8m

6.1.2 Force Coefficients

Drag force coefficient
Drag force, for a bluff body, is generated mainly due to the pressure difference between the front and rear of the truck. The force is positive when opposing the vehicle motion and is caused when there is a higher pressure at the front of the truck than at the rear. Figure 6.3 shows the drag coefficient experienced by the entire truck and the contributions due to the tractor and trailer.

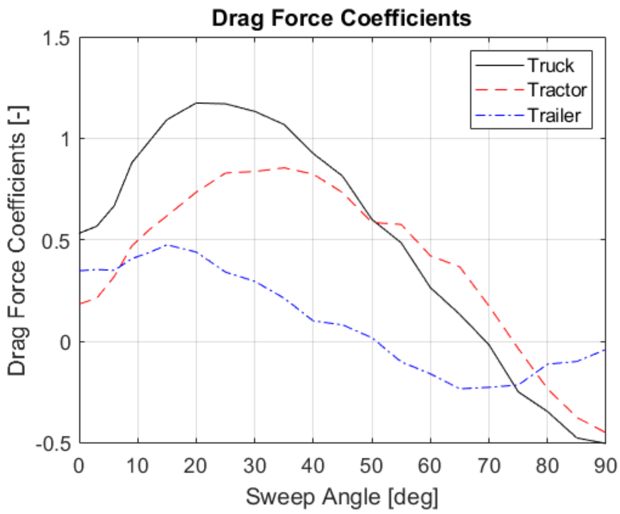

Figure 6.3: C_D obtained through STAR-CCM+

For the truck, the initial increase in the drag coefficients is due to an increasing pressure difference between the front of the tractor (stagnation area) and the rear of the trailer (wake region). After 20° yaw, the force coefficient starts to decrease and reaches zero at 70° yaw. The trend is followed until the minimum value is reached at 90° yaw. Figure 6.1 shows a shift in the stagnation region for varying yaw, while Figure 6.4 is helpful in visualizing the pressure in the x-direction for drag.

The tractor drag coefficient saw a greater change with respect to the yaw angle than the trailer drag coefficient. The rear surface of the tractor is majorly a low pressure region, while the front face turns into a low pressure region at higher yaw angles. When the yaw angle was increased, the air accelerated into the passage between the tractor and trailer, causing a further reduction in the low pressure region. However, post 40° yaw, the stagnation pressure no longer existed at the front of the tractor and as the yaw angle increased, a low pressure region was generated over the tractor face. It is observed that pressure is lower at the front face than the rear face of the tractor after 75° yaw, causing a negative drag across the tractor.

The front face of the trailer is partially exposed to the oncoming wind at lower yaw angles. The stagnation region increases up to a small yaw angle as the flow can enter the gap and hit the front surface. However, an angle exists where the flow acceleration overcomes the stagnation region. From 15° yaw onwards, the high pressure region reduced, thus, the drag coefficient decreased. The low pressure region in front of the trailer reduced beyond 70° yaw. Thus, the drag coefficient started to increase again.

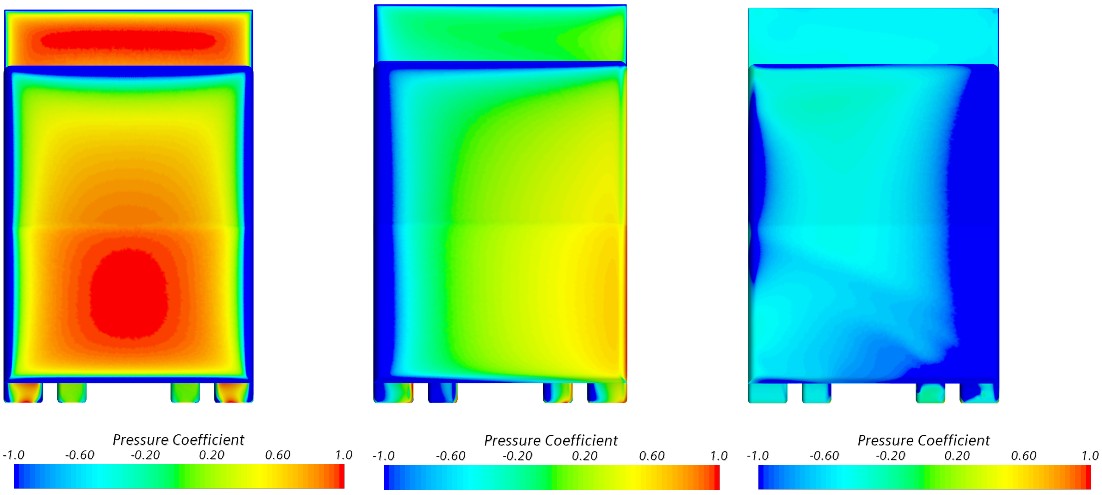

(a) $C_{p,front}$ for 0° yaw **(b)** $C_{p,front}$ for 45° yaw **(c)** $C_{p,front}$ for 90° yaw

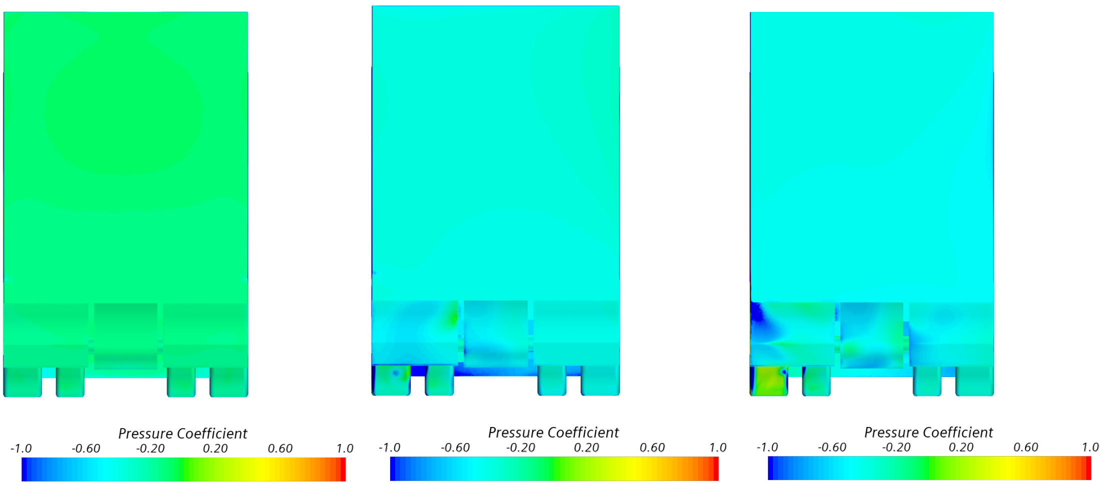

(d) $C_{p,rear}$ for 0° yaw **(e)** $C_{p,rear}$ for 45° yaw **(f)** $C_{p,rear}$ for 90° yaw

Figure 6.4: Pressure coefficients at the front and rear of the truck

Lift force coefficient

For a heavy vehicle like a truck, investigating lift force holds little importance. From Figure 6.6 is observed that the trailer heavily influences the truck lift coefficient. The lift coefficient of the truck is observed to increase until it peaks at 35° yaw, beyond which the lift coefficient starts to reduce. The detached flow over the trailer causes a low pressure region. As separation over the roof exists for all yaw angles, there is a positive lift coefficient for all yaw angles above 0° yaw. However, as the angle increases, the flow starts to accelerate under the trailer, this results in a reduction in pressure underneath the trailer. This can be seen from Figure 6.5 which shows the flow on plane at the centre of the trailer.

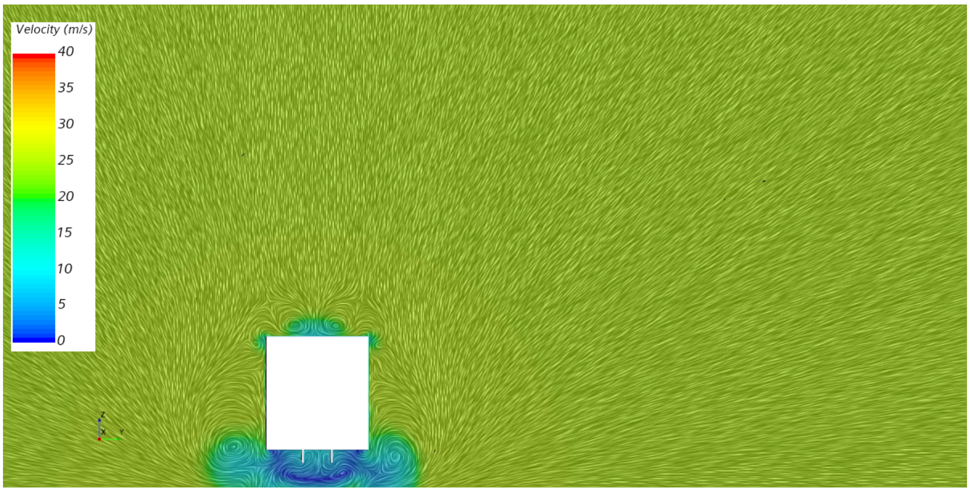

(a) 0° yaw

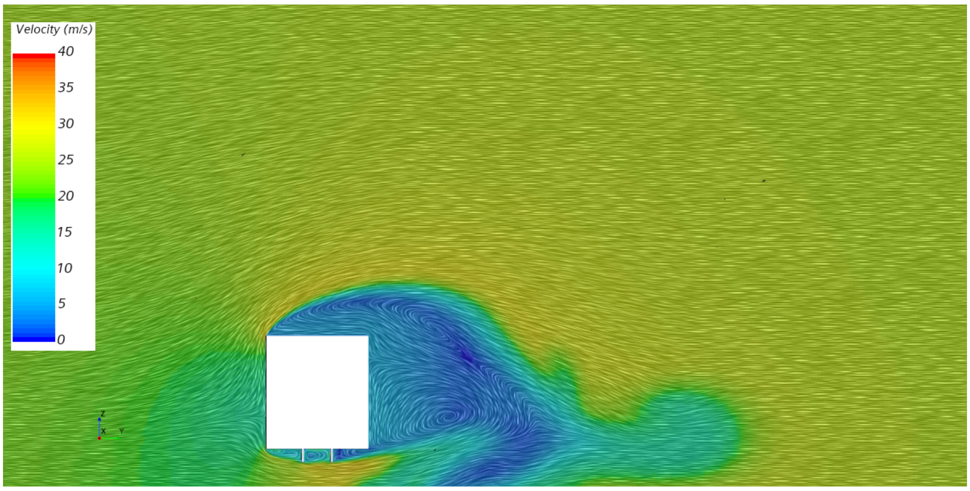

(b) 45° yaw

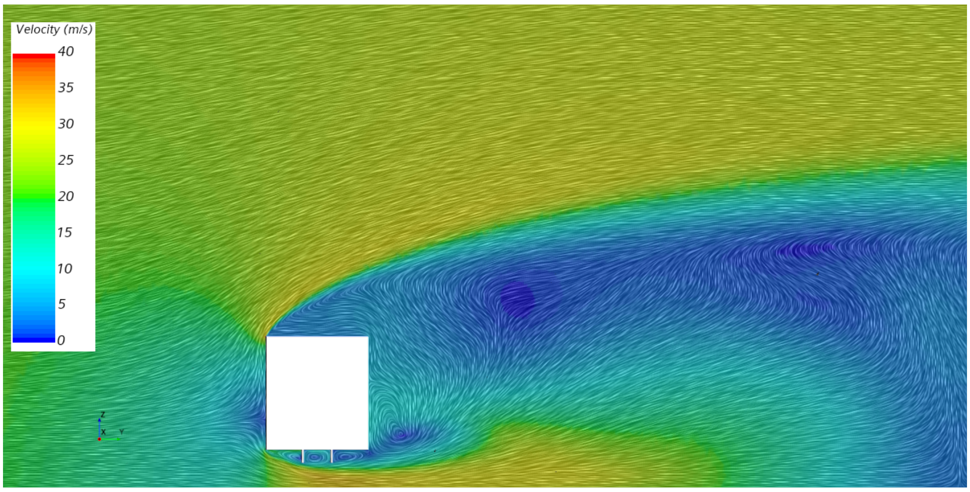

(c) 90° yaw

Figure 6.5: Rear view of velocity contours at the centre of the trailer

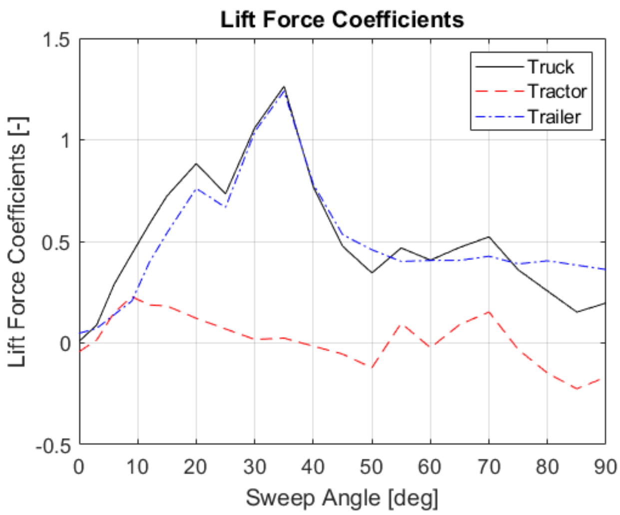

Figure 6.6: C_L obtained through STAR-CCM+

Side force coefficient

It is fair to assume that the side force experienced by the truck increases with increasing yaw angle. As seen in Figure 6.7, the side force generated by the trailer continues to increase with increasing yaw angle, however, the tractor side force decreases post 60° yaw. Thus, the side force coefficient for the truck plateaus after 75° yaw.

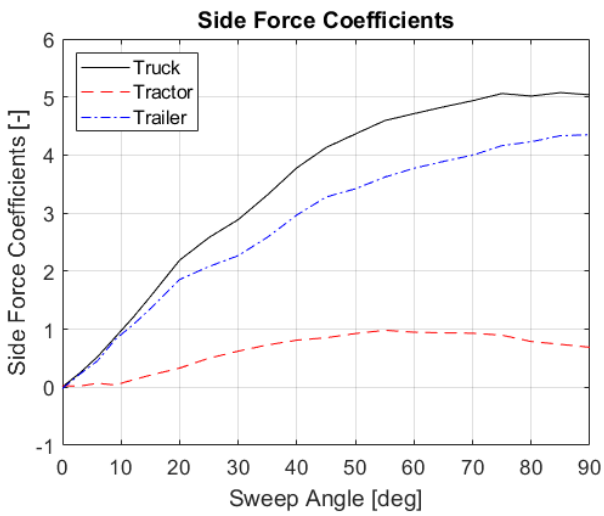

Figure 6.7: C_S obtained through STAR-CCM+

Figure 6.8 shows the wake region of the truck for two yaw angles: 60° and 65°. It is observed that the tractor wake is resolved individually up to 60° yaw and following that, the tractor wake mixes with the trailer wake. That is the yaw angle from where on the tractor side force coefficient starts to decrease.

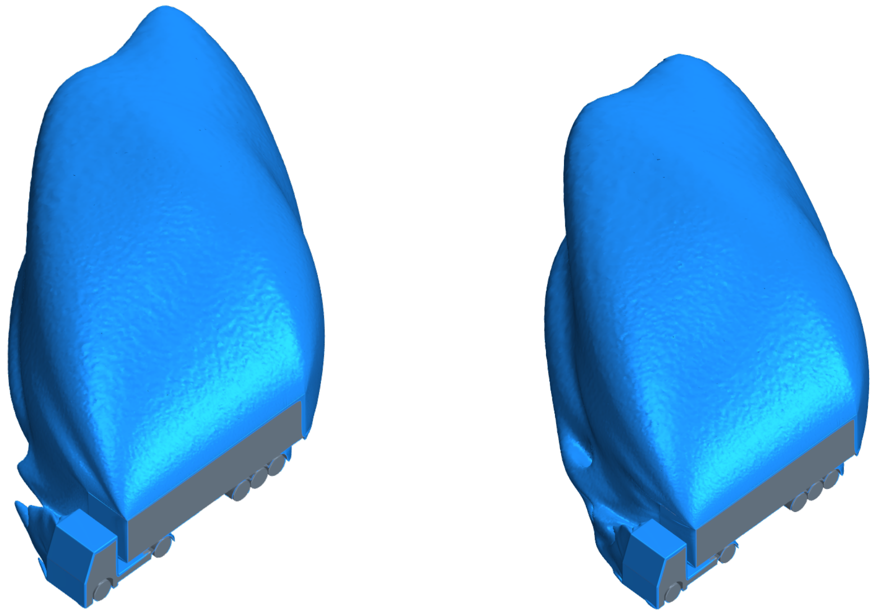

(a) 60° yaw **(b)** 65° yaw

Figure 6.8: Isosurface of $C_{p,total} = 0$

6.1.3 Moment Coefficients

All three moment coefficients, pitch, yaw and roll, are shown in Figure 6.9. The moment origin exists on the ground (Z $= 0\ m$), such that it is at the centre of the truck in the X and Y directions.

Pitch moment coefficient
The pitching moment indicates the load shift from along the lengthwise direction of the truck. It is the moment about the Y-axis and is a result of the drag and lift forces. Like the lift coefficient, the pitch coefficient contributes to the vertical loading which is not an important parameter for a truck. For lower yaw angles ($< 45°$), the pitch is positive, which corresponds to the drag and lift trends mentioned above. While a negative pitch is seen for higher yaw angles; indicating that the rear of the truck experiences more lift.

Yaw moment coefficient
The side and drag forces taken about the Z-axis result in a yaw moment. For lower yaw angles, the drag force is more dominant than the side force. The increasing yaw angle changes the centre of drag force actuation, which increases its contribution to the yaw moment. Thus, a negative yaw starts to develop. Once the side force starts to become dominant, the yaw increases as the rear of the truck contributes more to the side force.

Roll moment coefficient
A roll moment is caused due to the side and lift forces about the X-axis. As expected no roll moment is present at 0° yaw, it then increases in magnitude as the

yaw angles increases. This significant increase is due to a high pressure zone in the upwind region of the truck as the projected side area of the truck becomes larger.

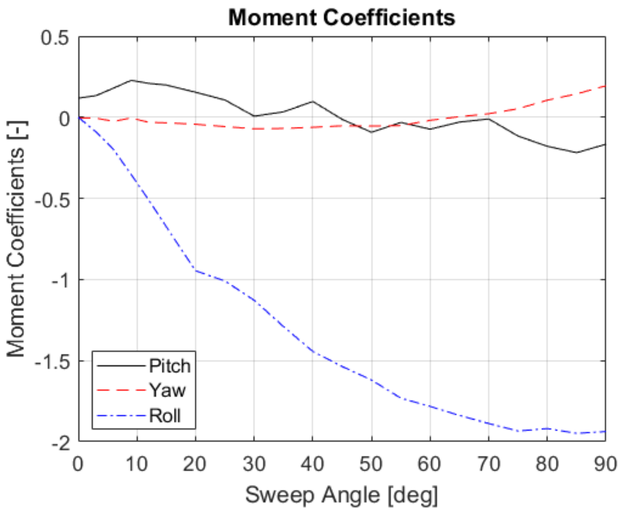

Figure 6.9: Moment coefficients from CFD for the base model

6.2 CFD & Wind-Tunnel Comparison for the Base Model

This section includes a comparison between the results of the CFD analysis and the Wind-tunnel testing.

6.2.1 Force Coefficients

Drag force coefficient

Figure 6.10a shows a similar trend for the drag force coefficients found from the CFD and wind-tunnel analyses respectively. However, there is a discrepancy between the two results, the wind-tunnel has a relatively stable offset from the CFD results up to 70° yaw. An explanation for this would be the differences in the testing conditions; in the wind-tunnel testing the ground was non-moving, the used mounting struts induced additional wakes, the wheels were non-rotating, and lastly the model was positioned such that the wheels did not touch the ground plate. These differences will have varying degrees of effect on the offset between the two graphs.

Lift force coefficient

From Figure 6.10b it can be seen that at 0° yaw, there is some discrepancy between the CFD and wind-tunnel results. The wind-tunnel results indicate down force being generated at low yaw angles, while the CFD analysis shows purely positive C_L values. The difference in using a stationary and moving ground for the the wind-tunnel testing and CFD analysis respectively could be an explanation for this. The exact effect of using a moving ground in the CFD analysis is hard to quantify, as other aspects, such as the increased ground clearance for the wind-tunnel model, could also have an effect on the lift coefficient. Presence of an inclination (pitch) of the model in the tunnel could also be a factor for the initial discrepancy. For both cases C_L increases with increasing yaw angles and peaks at around 35° with a C_L value of 1.3. After this peak, the flow velocity over the roof decreases and the lift forces decrease until 45° yaw. For larger angles the coefficient remains relatively stable.

Side force coefficient

The side force coefficient diverges beyond 35° as seen in Figure 6.10c. A prominent reason for this increasing divergence could be the mounting struts used in the wind-tunnel experiment. At low yaw angles these are still mostly hidden behind the wheels of the truck, however, as the yaw angle increases these struts become more exposed to the airflow.

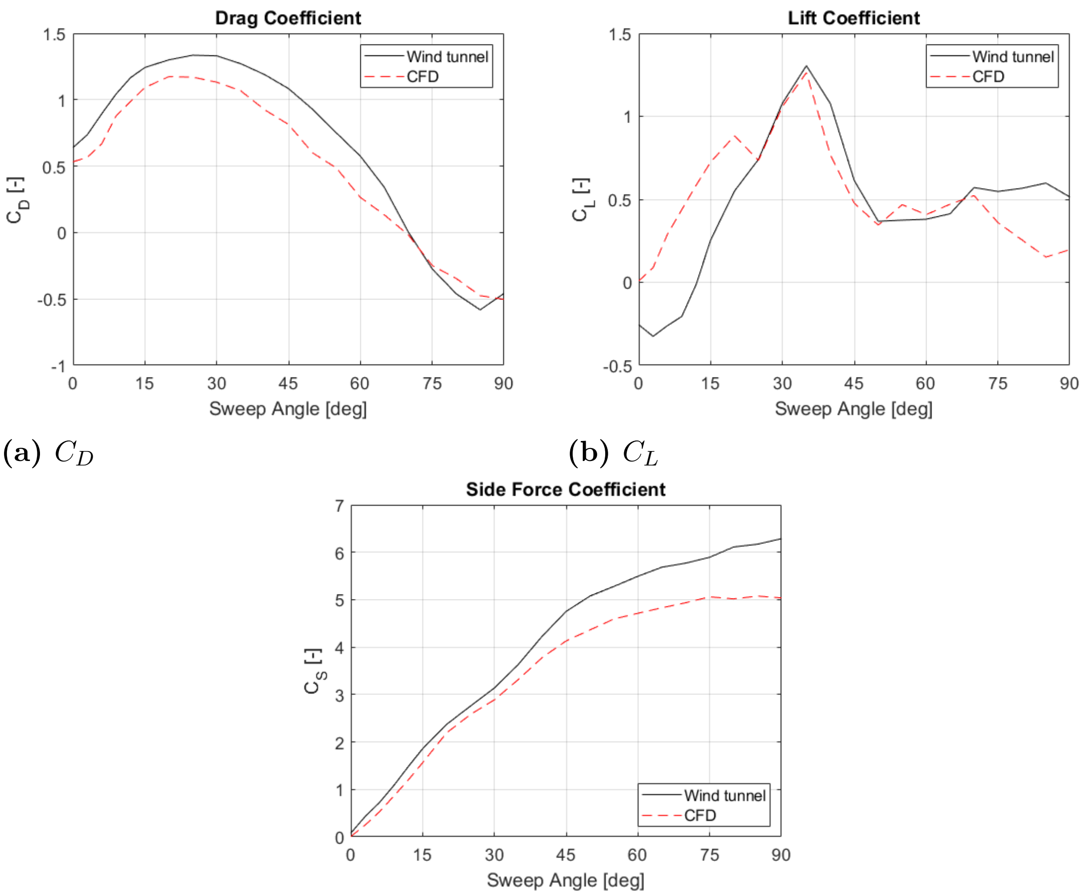

(a) C_D

(b) C_L

(c) C_S

Figure 6.10: Force coefficients compared between CFD and wind-tunnel results for the base model

6.2.2 Moment Coefficients

The trends of all moment coefficients from the wind-tunnel correlate to the respective CFD moment coefficients. However, the moment origin point from the wind-tunnel was unknown and approximated using the recorded forces. The CFD moment, taken about another point, was translated to match the wind-tunnel moment point. This process, along with the slight discrepancies in forces mentioned above results in the visible change in moment coefficients.

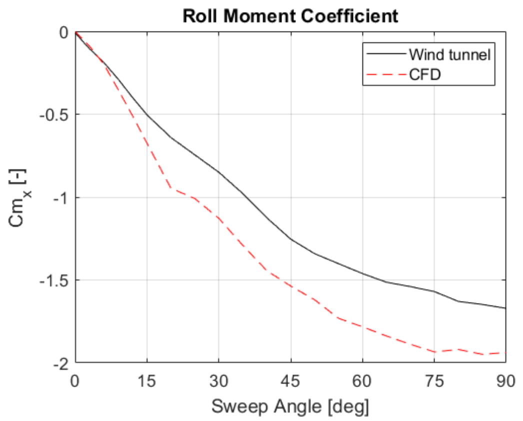

(a) C_{m_x}

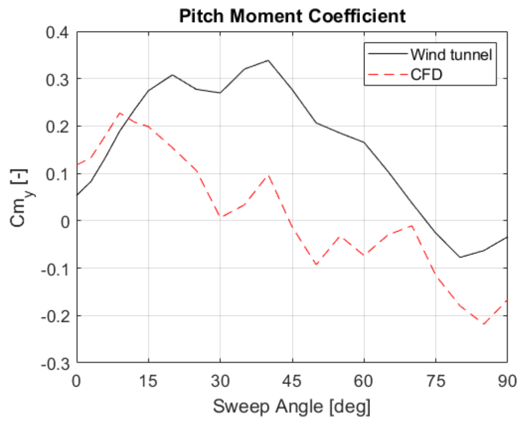

(b) C_{m_y}

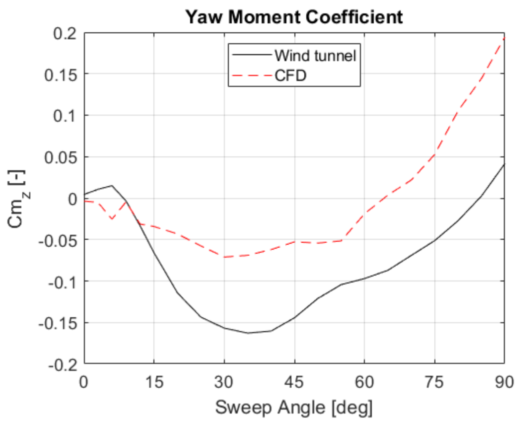

(c) C_{m_z}

Figure 6.11: Moment coefficients compared between CFD and wind-tunnel results for the base model

6.3 Wind-Tunnel Results for All Configurations

This section includes the presentation and discussion of the wind-tunnel experiment results. Firstly, the force coefficients are discussed, after which the moment coefficients results are outlined. The results include the yaw angle sweep for the four tested configurations. Lastly, symmetry of model in the wind-tunnel is analysed.

6.3.1 Force Coefficients

Drag force coefficient

From Figure 6.13a it can be seen that the base model with roof fairing experienced the least drag or it can be said the drag has been improved because of the continuity of the streamlined flow over the surfaces and the reducing of the stagnation area in front of the trailer area which exceeds above the tractor. The models with an increased gap show higher drag levels due to the larger re-circulation region between the tractor and trailer. The drag coefficients increases for all configurations up to around 25° yaw, after which it drops until it becomes negative at around 70° yaw. Figure 6.12 shows how the addition of roof fairing sends the flow over the gap and onto the trailer roof, which reduces the drag coefficient.

Figure 6.12: Base model with roof fairing during the wind-tunnel test for 0° yaw

Lift force coefficient

One can see that in Figure 6.13b all configurations have both negative as positive C_L values. Meaning that at low yaw angles, up to around 12°, down force is experienced by three configurations. For the "increased gap + roof fairing" setup this occurs later at approximately 18° yaw. After this, all configurations generate lift and all peak at around 35° yaw. The curves then dip down and rise back around 65°. The trend is similar for all the configurations.

Side force coefficient

From Figure 6.13c the trend can be seen that, with increasing yaw angle the side force increases as a greater part of the trucks surface gets exposed to the airflow. For all the four configurations the trend is linear from 0° to 45° and later it starts to get stable until 90°. The configuration with the increased gap between tractor and trailer along with a roof fairing has the better or lower side force experience. This is mainly to the increased gap size which allows a smoother airflow between the tractor and trailer. While the base model plus roof fairing configuration experiences higher side forces at higher yaw angles due to the small gap and the increased exposed area from the roof fairing. Overall the trend is very similar for the four configurations.

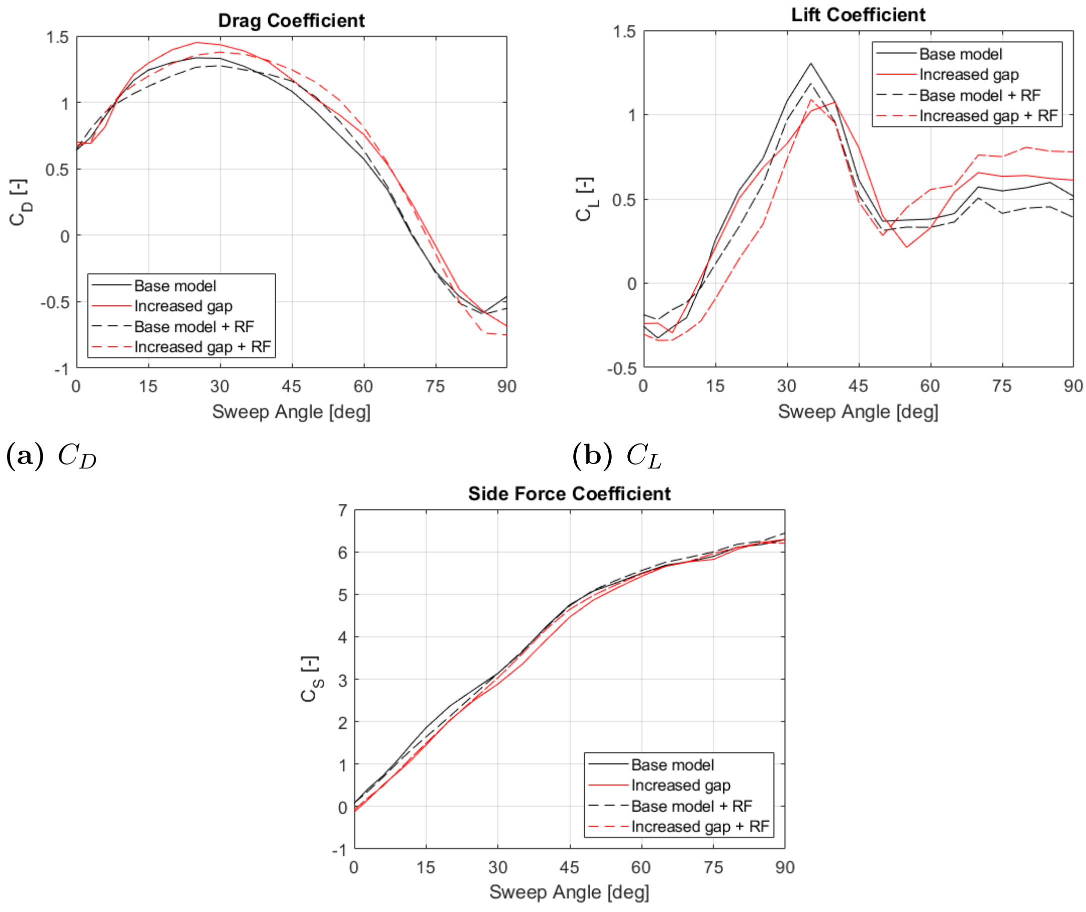

(a) C_D **(b)** C_L

(c) C_S

Figure 6.13: Force coefficients determined from wind-tunnel testing for different configurations

6.3.2 Moment Coefficients

Roll moment coefficient

In Figure 6.14a it can be seen that the coefficient of roll moment C_{m_x} increases almost linearly up-to 45° and further constantly increases until 90°. The rolling moment coefficient impacts the lateral direction weight distribution, the model becomes unstable with the increase in the value of roll moment. The roll moment is mainly dependent on the side force coefficient, as can be confirmed from the curves in Figure 6.13c. The trend is the same for all the four configurations.

Pitching moment coefficient

In Figure 6.14b the impact of yaw angle on the pitching moment of the truck model can be observed. The weight distribution gets affected due to pitching moment in longitudinal direction. It can be seen here that the pitching moment is higher for the increased gap configuration, while the base model plus roof fairing configuration has the lowest value. The pitching moment increases until 20° and then drops a bit and later there is a peak around 45° yaw. After 60° yaw all configurations show lesser pitching moment due to the airflow passing freely through the gap between tractor and trailer.

Yaw moment coefficient

The yaw moment is an important factor which decides the stability of the vehicle i.e. remaining in a straight path while moving. The coefficients of the yaw moment are shown in Figure 6.14c. One observation to be made is that at 0° yaw the moments coefficients are not zero, which would be expected for a perfectly symmetric model. A part of this offset could be caused by some asymmetry in the model, however this impact is likely fairly small. An error in the measurements could have a larger impact, the indicated yaw angle might not have been the exact yaw angle as this was hard to verify. However, all configurations do show a similar trend, there is a clear distinction between the two configurations with a standard tractor-trailer gap and the two configurations with an increased gap.

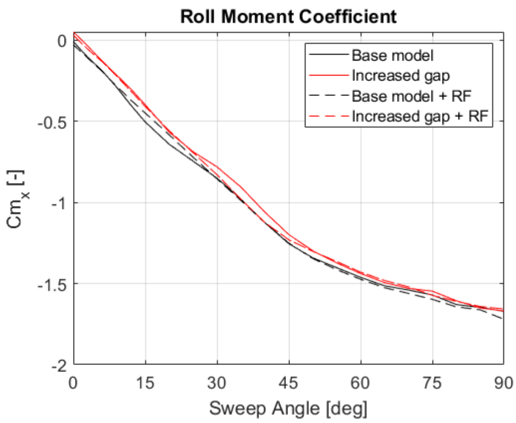

(a) C_{m_x}

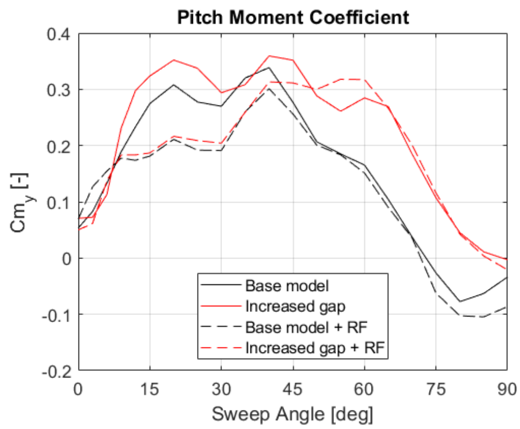

(b) C_{m_y}

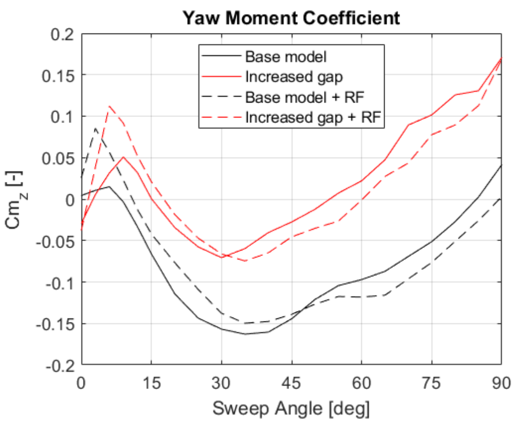

(c) C_{m_z}

Figure 6.14: Moment coefficients determined from wind-tunnel testing for different configurations

6.3.3 Symmetry of the Model

To see how symmetric the model used in the wind-tunnel was a symmetry test was performed. A number of yaw angles in the opposite direction were tested, as shown in Figure 6.15. Overall the model seems fairly symmetric, however some discrepancies can be seen in for example the C_L values. The coefficients of lift at 3° and -6 ° yaw is very similar. A possible explanation for this could be due to the indicated yaw angles not being the exact angles. As for all coefficients the values are offset between negative and positive yaw angles. Furthermore, the mounting of the model on the used mounting pins could have also effect the results, the model could have had an inclination in certain directions.

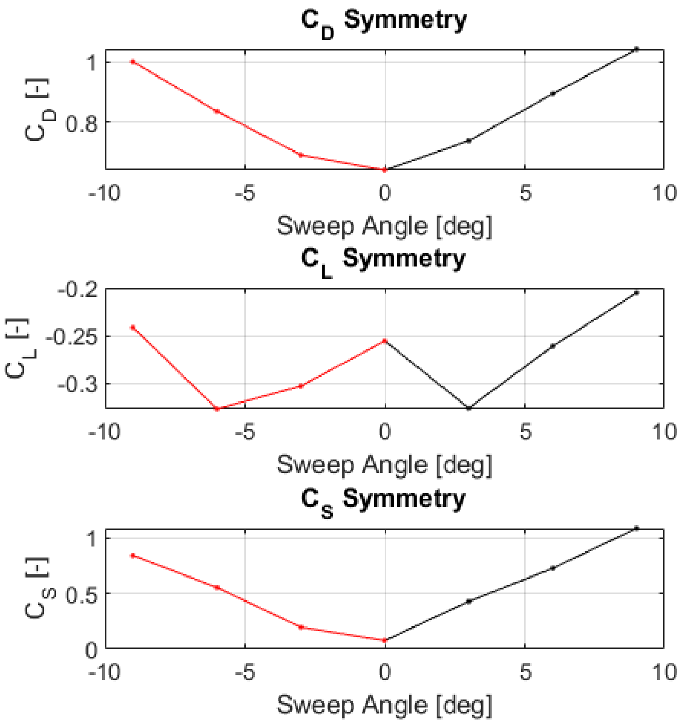

Figure 6.15: Symmetry analysis of the wind-tunnel base model

7

Important Considerations & Future Work

Concerning the CAD models, generating more triangles while converting 3D CAD files to STL file will give better overall accuracy and quality in the prints resulting in better mating of the parts.

During manufacturing of the physical model a number of points should be considered. Adding threaded inserts or making holes to fit the hex nuts in the 3D prints will provide better 'Torque-out' resistance and will give a much better overall clinching performance of the fasteners. Furthermore, orientation of the 3D parts on the print bed affects the accuracy and the warping of the prints. The parts must be placed on its flatter surface as much as possible to avoid layer shifting and vibrations during the printing process.

The simplifications made when designing the CAD, such as leaving out mirrors, radiator vents etc. affects the results of the analysis. However, most likely to a limited extend, since at crosswinds these parts would not play any key role. Hence it is acceptable to use this model for high yaw angles.

Regarding the wind-tunnel testing, one should take care to carefully take the measurements and check all necessary points. The results from the testing showed some discrepancies, most likely due to the mounting rods touching the moving plate in certain cases. Furthermore, the set yaw angles might not have been exact with respect to the airflow. Thus, one should pay extra attention when performing a sweep study. As the sweep study was performed back and forth these discrepancies could be accounted for.

For the CFD model, the effect of the road patch should be investigated. Currently an arbitrary size of $22m$*$8m$ is kept around the truck. The effect caused due to size variations is expected to be small, but still unknown. Another investigation that must be carried is how the truck velocity affects the side-wind force generation for a constant side-wind speed. This will help in deciding the speed limit for trucks on the floating bridge.

A number of further investigations into the effect of strong side winds on the stability of trucks could be performed in the future. This would for example include the testing of various aerodynamic alterations such as skirts covering the tractor-trailer gap, an American nose type or a boat tail. Furthermore, a more detailed investigation into the effect on vehicle dynamics, where other external conditions such as road conditions and driver capabilities are also included, would be highly beneficial.

8
Conclusion

This project aimed to study the stability of a generic simplified design of a truck under high crosswinds. The truck was evaluated with CFD simulations and a scaled model was tested in a closed-loop wind-tunnel, under a range of yaw angles. The physical model tested was modular, in order to investigate the influence of the addition of a roof fairing on the truck behavior.

Comparing the numerical and experimental results, it can be concluded that there was good correlation between them and, thus, they are valid. Any discrepancies found were attributed to the wind-tunnel testing setup, namely the absence of moving ground and rotating wheels, the existence of the mounting struts and the increased ground clearance that they caused.

It was observed that as the yaw angle increased the stability of the truck deteriorated. The main contributor of the side force was the trailer, as expected, while the increased gap between the tractor and the trailer had a beneficial impact on the magnitude of these forces. Additionally, at high yaw angles, the drag force became negative, peaking at 90°. As far as the use of the roof fairing is concerned, it caused reduction of the drag in lower yaw angles. However, as the angle increased the roof fairing was ineffective.

In conclusion, this project produced validated data of a generic truck under a range of yaw angles, which are available to determine and study the stability and the safety of these vehicle while driving on a floating bridge. However, since the experiments were implemented with a simplified scaled model and the CFD analysis was carried out with simple numerical models, the limitations of analysis should be taken into account. Further, CFD analysis and more extensive wind-tunnel testing could enhance the study.

Bibliography

[1] Bettle, J., Holloway, A.G.L., Venart, J.E.S., A computational study of the aerodynamic forces on a bridge in cross-wind. *Journal of Wind Engineering and Industrial Aerodynamics*, 91 (2003) 573–592

[2] Juhlin, M., & Eriksson, P. (2004), A Vehicle Parameter Study on Crosswind Sensitivity of Buses. *SAE Technical Paper Series*, (2004-01–2612).

[3] Torlund, P.,(1999). Experimentell undersökning av sidvindskänsligheten hos en modell av en tvåvåningsbuss i FFA's vindtunnel LT1. Report (in swedish), FFA TN 2000-05.

[4] Vdovin, A. (2020), Wind tunnel project instructions. *MTF236 - Road Vehicle Aerodynamics*, Chalmers University of Technology.

[5] William, Y.E., Mohamed, M., Oraby, W.A.H., Investigation of crosswind aerodynamics for road vehicles using CFD technique. *Eleventh International Conference of Fluid Dynamics*, 2013

[6] Zhang, Q., Su, C., Zhou, Y., Zhang, C., Ding, J., Wang, Y., Numerical Investigation on Handling Stability of a Heavy Tractor Semi-Trailer under Crosswind. *Applied Sciences*, 2020, 10(1), 3672.